Local environment dependent GGA+U method for accurate thermochemistry of transition metal compounds

Muratahan Aykol and C. Wolverton*

Department of Materials Science and Engineering, Northwestern University, Evanston, Illinois 60208, USA

(Received 16 May 2014; revised manuscript received 19 August 2014; published 2 September 2014; publisher error corrected 12 September 2014)

We present a framework to carry out highly accurate GGA+U thermochemistry calculations by deriving effective U values from experimental data. The U values predicted in this approach are applied to metal cations, and depend not only on (i) the chemical identity and the band to which the U correction is applied, but also on the local environment of the metal described by (ii) its oxidation state and (iii) the surrounding ligand. We predict such local environment dependent (LD) U values for the common oxidation states of 3d metals M = Ti, V, Cr, Mn, Fe, Co, and Ni in their oxides and fluorides. We implement the GGA/GGA+U mixing method [Jain *et al.* Phys. Rev. B **84**, 045115 (2011)] to establish the total energy compatibility among the GGA+U calculations involving M treated with different LD-U values. Using the presented framework, formation enthalpies of 52 transition metal bearing oxides (which are not used during the LD-U parametrization) are predicted with a remarkably small mean absolute error of ∼19 meV/atom, which is on the order of the experimental chemical accuracy. In addition, we present applications of the method in redox processes of important 3d-metal oxide and fluoride systems such as Li_xCoO_2, $Li_xV_6O_{13}$, Li_xFeF_3, and $VO_{1.5+x}$, and show that LD-GGA+U can overcome several drawbacks of using constant-U values in conventional GGA+U.

DOI: 10.1103/PhysRevB.90.115105 PACS number(s): 71.15.Dx, 71.27.+a, 65.40.G−, 81.30.Bx

I. INTRODUCTION

Quantum-mechanical design of novel materials, such as for lithium-ion batteries [1–6], hydrogen storage [7–10], thermoelectrics [11], structural metal alloys [12] or catalysis [13,14], among others, requires accurate and efficient description of thermochemistry of processes involving solid-state inorganic compounds, where density functional theory (DFT) has proven indispensable. However, when electron correlation effects dominate the DFT Hamiltonian, the spurious self-interaction of electrons in the formulation of the widely used exchange-correlation (XC) functionals of DFT, namely, the local density approximation (LDA) and generalized gradient approximation (GGA) [15], tend to overdelocalize electrons. This results in an inaccurate description of not only the electronic or magnetic properties, but also the thermochemistry of redox processes of strongly correlated materials. For example, in reactions involving open-shell first-row transition metal oxides with localized d electrons, the thermochemical accuracy of LDA or GGA diminishes relative to experiment [4,16–18]. This deficiency is more pronounced in reactions that involve transfer of electrons between significantly dissimilar environments such as between metallic and localized states [16,19]. A remedy to reduce the residual self-interaction is the so-called "LDA + U" method introduced by Anisimov *et al.* [20–22], where a Hubbard-type term is added to the density functional (LDA or GGA) that penalizes partial occupancies in correlated orbitals and subsequently localizes electrons. The LDA + U functional includes the onsite Coulomb (U) and exchange interaction (J) parameters, and in its simplified rotationally invariant formulations [23,24], U and J are combined to form an effective parameter $U_{\text{eff}} = U - J$ (hereafter, simply referred to as U).

The GGA+U functional can provide the same level of accuracy in redox reaction energies as the computationally demanding hybrid density functionals [18], but it requires an *ad hoc* input of the system-specific parameter U. Different methods of *ab initio* evaluation of U exist, such as constrained LDA (cLDA) [25,26], improved cLDA with linear-response approach [24], embedded cluster with unrestricted Hartree-Fock [27,28], and constrained random phase approximation [29,30]. But, these methods do not necessarily yield similar U values for a given system [24,31]. As an alternative, empirical selection of U to reproduce target properties such as band gaps, magnetic moments, lattice constants, or reaction energies is also common practice [16,32–34]. For redox reactions, Wang *et al.* [16] showed that if the errors associated with the GGA representation of diatomic molecules [16,35] are separated from the errors stemming from correlation effects *a priori*, one can find a reasonable U value (a constant U for a given redox pair) that reproduces the experimental reaction energies. One has to inevitably use such a constant U for all different compounds of M in a conventional GGA+U based thermochemical study [4,16,36–38] since the total energies at different U values cannot be compared directly.

Physically, the onsite Coulomb interactions depend on the local environment of the transition metal atom M, and hence one should expect U to differ between environments where M has different electronic states (e.g., described by observables such as the oxidation state, spin state, etc.) and is coordinated with different ligands [4,24]. Use of a constant U for all M in different local chemistries can often lead to inaccuracies, especially in reactions where the electronic character of the phases involving M are considerably different [37,38]. For example, Jain *et al.* [38] showed that conventional GGA+U, despite the fitted O_2 chemical potential, yields a mean absolute relative error over 21% in formation enthalpies of d-block metal oxides, mostly resulting from the application of U on metallic elemental references. Constant-U GGA+U error

*c-wolverton@northwestern.edu

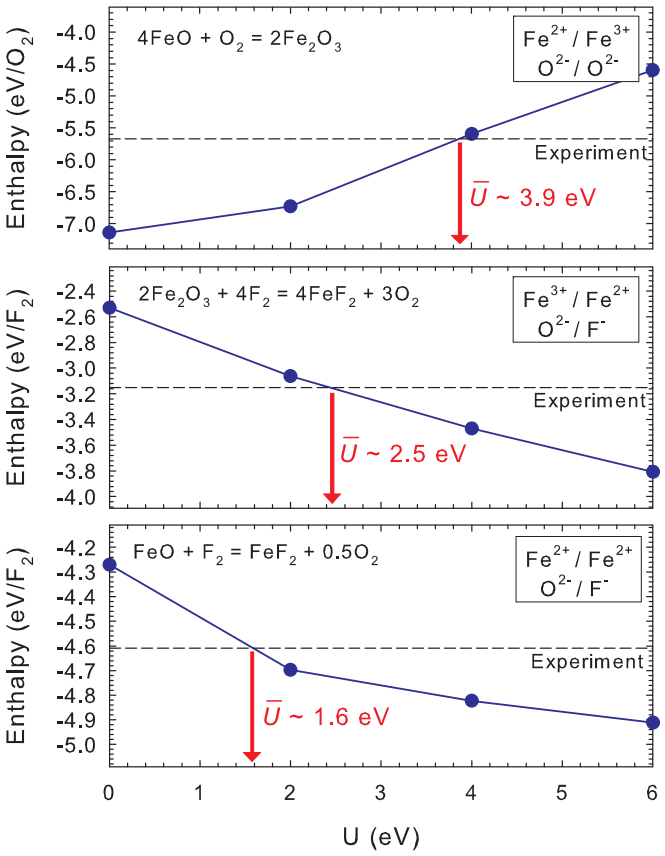

FIG. 1. (Color online) Finding the constant U value ($\bar{U}$) where GGA+U enthalpy of the reaction matches the experimental value for a sample set of three reactions among FeO, Fe_2O_3, and FeF_2 using the method of Wang *et al.* [16]. The sample reactions shown clearly require significantly different $\bar{U}$ values. The O_2 and F_2 chemical potentials are corrected in advance using the corrections given in Sec. III A.

can still persist in reaction enthalpies even in the absence of elemental phases. For instance, as shown in Fig. 1, while a U of ∼3.9 eV can accurately reproduce the experimental enthalpy of the reaction $4FeO + O_2 \rightarrow Fe_2O_3$, use of the same U in the reaction $FeO + F_2 \rightarrow FeF_2 + 0.5O_2$ leads to an error of ∼18 kJ, which is significant relative to the typical experimental accuracy of ∼4 kJ. In fact, the experimental enthalpy of the latter reaction can be reproduced using a significantly different U of ∼1.6 eV. As a further example where even no diatomic molecules are involved, the experimental enthalpy of the reaction $V_2O_3 + V_2O_5 \rightarrow 4VO_2$ cannot be reproduced at any constant-U value (see the Supplemental Material [39]). A widely used U of ∼3.1 eV for vanadium oxides results in an error of ∼17 kJ in the enthalpy in this case. A "reasonably selected" constant U for GGA+U thermochemistry, therefore, may not adequately represent a multivalent M in different solid phases with dissimilar local environments.

In this study, we present a method to find U values that depend on the chemical identity of the metal M, as well as characteristics pertaining to its local environment in a compound; namely, its oxidation state ($a+$) and surrounding ligand (X). The method is based on formulating a relation between such local environment dependent (LD) U values ($U^X_{M^{a+}}$) and the constant U values of M fitted using experimental reaction energies. We apply the method to predict LD-U values for thermochemical GGA+U calculations of oxides and fluorides of first-row transition metals Ti, V, Cr, Mn, Fe, Co, and Ni, using mainly their binary compounds. The total energy compatibility among calculations involving M at different $U^X_{M^{a+}}$ values is realized by implementing the GGA/GGA+U mixing method of Jain *et al.* [38]. We validate the transferability of the $U^X_{M^{a+}}$ values to similar local environments by showing that LD-GGA+U yields a mean absolute error of ∼19 meV/atom in predicting the formation enthalpies of a test set of 52 ternary and mixed-valence binary metal compounds. We further demonstrate applications of the LD-GGA+U method in case studies on challenging mixed-valence redox processes in Li-ion batteries and phase diagrams. The LD-GGA+U formalism can correct several deficiencies of using a constant-U value for M in conventional GGA+U thermochemistry studies. The method we present can be easily applied to new systems, as it only requires performing regular GGA+U calculations.

II. LOCAL ENVIRONMENT DEPENDENT GGA+U METHOD

A. Calculating the local environment dependent Hubbard U

Using a reaction between two different compounds of a metal M, a constant-U value (hereafter denoted as $\bar{U}$) can be determined via a procedure of fitting to experimental data [16]. We illustrate this procedure for a sample set of three Fe compounds FeO, Fe_2O_3, and FeF_2 in Fig. 1. For the three different reactions that we can devise among these compounds, we find three significantly different $\bar{U}$ values. We hypothesize that if one can establish a relation between such $\bar{U}$ of a reaction, and the unknown $U^X_{Fe^{a+}}$ values of the compounds in that reaction, these $U^X_{Fe^{a+}}$ values can be recovered. In this particular example, we have three unknown $U^X_{Fe^{a+}}$ values and three relations; i.e., $f(U^O_{Fe^{2+}}, U^O_{Fe^{3+}}) \approx 3.9$ eV, $f(U^O_{Fe^{3+}}, U^F_{Fe^{2+}}) \approx 2.5$ eV, and $f(U^O_{Fe^{2+}}, U^F_{Fe^{2+}}) \approx 1.6$ eV. When the relation f is defined, one can easily invert these equations to find $U^O_{Fe^{2+}}$, $U^O_{Fe^{3+}}$, and $U^F_{Fe^{2+}}$. In this section, we generalize the procedure outlined above, and also propose a functional form for f to use in this model that allows extracting the LD-U values.

In the first step, we start by defining the chemical space of interest and selecting compounds that adequately sample this chemical space, i.e., common oxidation states of M are included in our set of selected compounds. To illustrate the method, we choose oxides and fluorides of M in this work, but the method should be broadly applicable in other chemical spaces as well. For n number of selected compounds, enumerating all possible reactions among pairs of compounds in this set, one can write $p = n(n-1)/2$ number of different reactions in the following generic form:

$$M^{a+}X^{x-}_{a/x} + \frac{b}{2y}Y_2 \rightarrow M^{b+}Y^{y-}_{b/y} + \frac{a}{2x}X_2. \qquad (1)$$

Here, $a+$ and $b+$ are the valences of M in compounds $MX_{a/x}$ and $MY_{b/y}$, respectively. Similarly, $x-$ and $y-$ are the valences of ligands X and Y, respectively. If $a = b$ (i.e.,

a single oxidation state of M), X^{x-} and Y^{y-} must indicate different ligands, and if $a \neq b$ (i.e., multiple oxidation states of M), they can be different or identical ligands. For each reaction, we use the method by Wang *et al.* [16] to find a $\bar{U}$. In that method, one first isolates the GGA errors in the chemical potentials of molecules of ligands (here, O_2 and F_2) by fitting them separately to formation reactions of simple metal compounds (see Sec. II B for further details). Then, for the ith reaction in the form of Eq. (1), the enthalpy of the reaction (ΔH_i^{calc}) is calculated as a function of U with the conventional GGA+U scheme (applying the same U to M in both compounds). The value $\bar{U}_i$ can be found using

$$\Delta H_i^{\text{calc}}(\bar{U}_i) = \Delta H_i^{\text{expt}} = \Delta H_f^{\text{expt}}[MX_{a/x}] - \Delta H_f^{\text{expt}}[MY_{b/y}], \quad (2)$$

where ΔH_i^{expt} is the experimental reaction enthalpy. ΔH_i^{expt} can often be calculated using the experimental formation enthalpies (ΔH_f^{expt}) of reactants and products. For n compounds, the above procedure will yield p number of different $\bar{U}_i$ values (assuming a $\bar{U}_i$ can be found for each reaction). With a minimum of three compounds, we will have $p \geqslant n$, i.e., the number of unknown LD-U values ($U^X_{M^{a+}}$) will be less than or equal to the number of reactions for which $\bar{U}_i$ is known. Therefore, once we formulate the relation f between $\bar{U}_i$, and $U^X_{M^{a+}}$ and $U^Y_{M^{b+}}$ of the compounds in the corresponding reaction, we can invert these p number of relations to find the unique LD-U values.

We start our search for such a relation f by realizing that as long as the constant-U GGA+U energy of Eq. (1) is a monotonic function of U (which is often the case), $\bar{U}_i$ can be expected to lie between $U^X_{M^{a+}}$ and $U^Y_{M^{b+}}$. Supporting evidence is seen in the work by Zhou *et al.* [4], where the experimental redox potentials of spinel, olivine, and layered Li-ion battery cathodes were reproduced at U values that lie between the unique U values (calculated with a cLDA approach) of lithiated/delithiated compounds in the reactions. Then, the next question is where exactly $\bar{U}_i$ is located in the interval enclosed by $U^X_{M^{a+}}$ and $U^Y_{M^{b+}}$. We approach this problem with a method analogous to determination of the phase boundaries in magnetic phase diagrams of model Hubbard Hamiltonians [40–42] where U is treated as an intensive thermodynamic variable. For the compounds in the ith reaction, we assume that initially there are two isolated systems, one of which has the compound $MX_{a/x}$ at $U^X_{M^{a+}}$ and the other one has the compound $MY_{b/y}$ at $U^Y_{M^{b+}}$. Since dE/dU is always positive, changing these unique U values to $\bar{U}_i$ will result in an increase in E of one of the compounds (which has the smaller U) and a decrease in that of the other compound (which has the larger U). Then, if we assume that the energy increase in one compound compensates the energy decrease in the other one to conserve the total energy when both compounds are brought from their unique U values to a common U of $\bar{U}_i$, we can write

$$E_{MX_{a/x}}(\bar{U}_i) + E_{MY_{b/y}}(\bar{U}_i) = E_{MX_{a/x}}\left(U^X_{M^{a+}}\right) + E_{MY_{b/y}}\left(U^Y_{M^{b+}}\right). \quad (3)$$

Equation (3) relates $\bar{U}_i$ of the ith reaction to $U^X_{M^{a+}}$ and $U^Y_{M^{b+}}$. This approximation requires knowing E as a function of U for each compound, which can be readily obtained with GGA+U (see Appendix A). The only unknowns that remain in Eq. (3) are $U^X_{M^{a+}}$ and $U^Y_{M^{b+}}$. Given p number of Eq. (3)'s, solving for these unique U values is an exactly determined problem if $p = n$ or an overdetermined optimization problem for $p > n$, for which we prefer the least-squares optimization.

B. Total energy compatibility for LD-GGA+U calculations

To be able use the different $U^X_{M^{a+}}$ for M in GGA+U based thermochemistry, we must establish compatibility among the total energies of phases involving M treated with different $U^X_{M^{a+}}$ as well as those preferentially treated with GGA. The recently introduced methods such as the GGA/GGA+U mixing by Jain *et al.* [38] or the fitted elemental reference energies (FERE) by Stevanović *et al.* [43] (based on the method by Lany [44]) already provide the necessary basis to use the LD-U values in GGA+U thermochemistry. Here, first we briefly summarize these methods, and then describe the implementation of a similar approach into the LD-GGA+U framework.

In both GGA/GGA+U mixing and FERE methods, each phase in the following formation reaction for the compound $MX_{a/x}$ is allowed to be treated with the preferred functional (GGA or GGA+U):

$$M + \frac{a}{2x}X_2 \rightarrow MX_{a/x}. \quad (4)$$

The compatibility of total energies from different functionals is then realized by including energy corrections in the formation enthalpy expression as

$$\Delta H_f^{\text{calc}}[MX_{a/x}] = E^{\text{GGA+}(U)}_{MX_{a/x}} - \mu^{\text{GGA+}(U)}_M - \frac{a}{2x}\mu^{\text{GGA}}_{X_2} - \underbrace{\left(\Delta\mu_M + \frac{a}{x}\Delta\mu_X\right)}_{\text{Corrections}}. \quad (5)$$

Here, $E^{\text{GGA+}(U)}_{MX_{a/x}}$ is the GGA+U total energy of $MX_{a/x}$ (since the FERE method can also be applied to compounds of $M \notin d$-block, one could also use the GGA energy for such compounds). $\mu^{\text{GGA+}(U)}_M$ is the chemical potential of M in its elemental state (for which Jain *et al.* [38] used GGA, and Stevanović *et al.* [43] used GGA+U if $M \in d$-block). $\mu^{\text{GGA}}_{X_2}$ is the chemical potential of the X_2 molecule. The energy corrections per M and per X atoms are denoted as $\Delta\mu_M$ and $\Delta\mu_X$, respectively. In each method, these corrections are optimized such that ΔH_f^{calc} matches ΔH_f^{expt} for a selected set of formation reactions. In the FERE method, $\Delta\mu_M$ and $\Delta\mu_X$ are globally optimized using a large set formation enthalpies of compounds of s-, p-, and d-block metals. In the GGA/GGA+U mixing method, $\Delta\mu_X$ is optimized in advance using formation reactions of simple metal compounds and assuming $\Delta\mu_M = 0$ (similar to the method of fitting $\Delta\mu^{\text{fit}}_{O_2}$ in Refs. [16,35]). Then, $\Delta\mu_M$ is fitted to the formation reactions of a set of $MX_{a/x}$ compounds to find an average $\Delta\mu_M$. Energy correction methods for GGA+U calculations are already implemented in online DFT databases [45–47]. Using the GGA/GGA+U mixing and FERE methods, formation enthalpies of ternary compounds can be accurately predicted with mean absolute errors (MAEs) on the order of ~45–50 meV/atom [38,43].

In the LD-GGA+U framework, we adopt a method similar to the GGA/GGA+U mixing method of Jain *et al.* [38]. Here, we briefly provide an interpretation for the physical meaning of such energy corrections for M that is consistent with the rest of our framework. We hypothesize that an approach to achieve the energy compatibility is to bring the energies of compounds of M from the GGA+U level $U^X_{M^{a+}}$ to the $U \to 0$ limit. The change in the total energy of $MX_{a/x}$ with this process can be defined as $\Delta\mu^X_{M^{a+}}$. Apparently, the limit $U \to 0$ here does not correspond to GGA with $U = 0$ (which we are already trying to correct by applying U). Instead, $U \to 0$ can be assumed as a hypothetical GGA state with the "correct electronic structure" captured at $U^X_{M^{a+}}$. The total energy at this hypothetical $U \to 0$ limit ($E^{U\to0}_{MX_{a/x}}$) can be written as

$$E^{U\to0}_{MX_{a/x}} = E_{MX_{a/x}}\left(U^X_{M^{a+}}\right) - \Delta\mu^X_{M^{a+}}. \tag{6}$$

We can find $E^{U\to0}_{MX_{a/x}}$ by fitting the calculated formation enthalpy of $MX_{a/x}$ to the experimental value as

$$\begin{aligned}\Delta H_f^{\text{expt}}[MX_{a/x}] &= \Delta H_f^{\text{calc}}[MX_{a/x}] \\ &= E^{U\to0}_{MX_{a/x}} - \mu_M^{\text{GGA}} - \frac{a}{2x}\mu^{\text{fit}}_{X_2},\end{aligned} \tag{7}$$

where we assume the GGA representation of elemental M and the separately fitted X_2 chemical potential ($\mu^{\text{fit}}_{X_2} = \mu^{\text{GGA}}_{X_2} + 2\Delta\mu_X$) require no further corrections. In other words, the discrepancy between GGA and experimental formation enthalpies of $MX_{a/x}$ is assumed to result from the correct $E^{U\to0}_{MX_{a/x}}$ being unknown. Inserting Eq. (6) into Eq. (7), $\Delta\mu^X_{M^{a+}}$ corresponding to $U^X_{M^{a+}}$ can be found as

$$\begin{aligned}\Delta\mu^X_{M^{a+}} &= E_{MX_{a/x}}\left(U^X_{M^{a+}}\right) - \mu_M^{\text{GGA}} \\ &\quad - \frac{a}{2x}\mu^{\text{fit}}_{X_2} - \Delta H_f^{\text{expt}}[MX_{a/x}].\end{aligned} \tag{8}$$

In analogy with $U^X_{M^{a+}}$, we assume that a $\Delta\mu^X_{M^{a+}}$ value is transferable to other compounds where M has a similar local environment defined by $a+$ and X. We can, therefore, obtain the corrected total energy of a given compound as

$$E^{U\to0}_{\text{compound}} = E^{\text{GGA+}U}_{\text{compound}} - \sum_{M^{a+}} n^X_{M^{a+}}\Delta\mu^X_{M^{a+}}, \tag{9}$$

where $n^X_{M^{a+}}$ is the number of M^{a+} ions that $U^X_{M^{a+}}$ is applied, and the summation is over all different types of M^{a+} in the compound. Total energies of compounds must be corrected as above to ensure energy compatibility among all LD-GGA+U calculations.

C. Practical use of LD-GGA+U: A recipe

Here, we summarize the steps involved in a practical application of the LD-GGA+U method:

(1) Reactions and reaction energies to train LD-GGA+U parameters: To describe M in the chemical space of interest (e.g., oxides, fluorides, sulfides, phosphates, etc.), a set of compounds should be selected such that they adequately represent the common oxidation states of the metal M (e.g., 2+ and 3+ for Fe) coordinated with the ligands present in the chemical space (such as O^{2-}, F^-, etc.). Using these compounds of M, reactions in the form of Eq. (1) are written. Experimental energies of all these reactions must be known; therefore, the compounds should be chosen accordingly. For species such as O_2 or F_2 that would appear in the reactions, systematic GGA errors should be corrected in advance using the method of Wang *et al.* [16,35].

(2) Find $E_{MX_{a/x}}(U)$: For each compound, a series of regular GGA+U calculations are performed at several U values to find the variation of the total energy $E_{MX_{a/x}}$ with U. The functional form of $E_{MX_{a/x}}(U)$ can often be adequately represented by a quadratic polynomial fitted to the calculated $E_{MX_{a/x}}$ at discrete U values with intervals of 1–2 eV (see Appendix A).

(3) Find $\bar{U}_i$: For each reaction determined in the first step, $\bar{U}_i$ (i.e., the constant-U value where conventional GGA+U reaction enthalpy matches the experimental counterpart) is found using Eq. (2).

(4) Find $U^X_{M^{a+}}$: For each reaction where a $\bar{U}_i$ can be found [i.e., Eq. (2) has a solution, see Appendix B], a corresponding equation in the form of Eq. (3) relates $\bar{U}_i$ to $U^X_{M^{a+}}$ and $U^Y_{M^{b+}}$. By using the analytic form of total energies $E_{MX_{a/x}}(U)$ found in step 2, one then simply solves this series of equations to get $U^X_{M^{a+}}$ values. If the number of $\bar{U}_i$ values (i.e., equations) is equal to the number of $U^X_{M^{a+}}$ values (i.e., unknowns), the equations can be solved exactly. If the number of $\bar{U}_i$ values (i.e., equations) is greater than the number of $U^X_{M^{a+}}$ values (i.e., unknowns), $U^X_{M^{a+}}$ can be found by an optimization method such as least-squares fitting.

(5) Find $\Delta\mu^X_{M^{a+}}$: For each $U^X_{M^{a+}}$ calculated in step 4, the corresponding energy correction factor $\Delta\mu^X_{M^{a+}}$ is calculated using Eq. (8).

The LD-GGA+U parameters $U^X_{M^{a+}}$ and $\Delta\mu^X_{M^{a+}}$ obtained with the procedure above are used to calculate the corrected total energy of a given compound of M using Eq. (9). These total energies can then be used to compute thermochemical properties such as reaction energies or phase stabilities.

III. METHODS

A. First-principles calculations

All first-principles calculations were carried out with the Vienna *ab initio* simulation package (VASP) [48–51]. The generalized gradient approximation (GGA) of Perdew-Burke-Ernzerhof (PBE) to exchange-correlation functional [52,53] was used with projector augmented wave (PAW) potentials [54]. To ensure convergence, a plane-wave basis set cutoff energy of 520 eV and an approximate k-point density of 8000 per reciprocal atom were used [55]. The rotationally invariant approach of Dudarev *et al.* [23] was used for GGA+U calculations. For all compounds employed in the LD-U prediction, we considered the experimental magnetic structures listed in Table I, and also tried different spin initializations (high and low) when possible. We observed that if a ferromagnetic (FM) spin configuration is not the ground state [but instead, for example, antiferromagnetic (AFM) or ferrimagnetic (FiM) configuration leads to a lower-energy solution], calculations started with FM spins are more prone to being trapped in local minima of GGA+U [76]. This trapping often leads to too high GGA+U energies, and therefore, inconsistencies in the U prediction step. Thus, if no experimentally reported magnetic structure is available, we tried both ferromagnetic and nonmagnetic calculations, as well as possible AFM or

TABLE I. Experimental enthalpy of formation at absolute zero temperature (ΔH_f^{expt}), space group, ICSD No., and magnetic structure of binary 3d-metal oxides and fluorides used in local environment dependent U predictions.

Compound	ΔH_f^{expt} (eV/atom)	Source[a]	Space group	ICSD No.	Magnetic structure[b]
CoO	−1.234	Ja	$Fm\bar{3}m$	29049	AFM [63]
Co_3O_4	−1.327	Ja	$Fd\bar{3}m$	27497	AFM [64]
CoO_2	−0.975	R1	$R\bar{3}m$ (O3)		NM
CoF_2	−2.323	R2	$P4_2/mnm$	26604	AFM [65]
CoF_3	−2.043	e-Ja	$R\bar{3}cR$	16672	AFM [66]
Cr_2O_3	−2.340	Ja	$R\bar{3}cH$	25781	AFM [67]
CrO_2	−2.058	e-Ba	$P4_2/mnm$	202837	FM [68]
CrO_3	−1.508	e-Ku	$C2cm$	24043	DM
CrF_2	−2.687	R3	$P12_1/n1$	31827	AFM [69]
CrF_3	−2.997	e-Ku	$R\bar{3}cR$	31828	AFM [66]
CrF_4	−2.581	e-Ba	$P4_2/mnm$	78778	Unknown [70]
FeO	−1.414	e-Ja	$Fm\bar{3}m$	31081	AFM [63]
Fe_2O_3	−1.698	Ja	$R\bar{3}cH$	15840	AFM [67]
FeF_2	−2.479	R3	$P4_2/mnm$	9166	AFM [65]
FeF_3	−2.628	R4	$R\bar{3}cR$	41120	AFM[66]
MnO	−1.995	e-Ku	$Fm\bar{3}m$	18006	AFM [63]
Mn_2O_3	−1.978	e-Ku	$Pcab$	9090	AFM [71]
MnO_2	−1.786	e-Ku	$P4_2/mnm$	393	AFM [72]
MnF_2	−2.954	R5	$P4_2/mnm$	14142	AFM [65]
MnF_3	−2.770	e-Ba	$C12/c1$	19080	AFM [66]
MnF_4	−2.239	R6	$I4_1/a$	62068	Unknown
NiO	−1.224	e-Ku	$Fm\bar{3}m$	9866	AFM [63]
$BaNiO_3$	−1.889	R7	$P6_3/mmc$	175	Unknown
NiF_2	−2.268	e-Ku	$P4_2/mnm$	9168	AFM [65]
Ti_2O_3	−3.135	Ja	$R\bar{3}cR$	6095	NM [73]
TiO_2	−3.247	Ja	$P4_2/mnm$	9161	DM
TiF_3	−3.713	e-Ja	$R\bar{3}cR$	16649	FM
TiF_4	−3.414	Ja	$Pnma$	78737	DM
VO	−2.227	Ja	$Fm\bar{3}m$	28681	AFM [74]
V_2O_3	−2.516	Ja	$R\bar{3}cR$	33641	AFM [75]
VO_2	−2.450	Ja	$P12_1/c1$	34033	NM [74]
V_2O_5	−2.282	Ja	$Pmnm$	15798	DM
VF_3	−3.272	R8	$R\bar{3}cR$	30624	FM [66]
VF_4	−2.904	e-Ba	$P12_1/n1$	65785	Unknown

[a]Ja: Janaf at 0 K; e-Ja: Janaf extrapolated to 0 K; Ku: Kubaschewski; e-Ku: Kubaschewski extrapolated to 0 K; e-Ba: Barin extrapolated to 0 K; R1: Ref. [56]; R2: Ref. [57], extrapolated to 0 K with Ku data; R3: Ref. [58], extrapolated to 0 K with Ku data; R4: average of Ja and Ref. [59] extrapolated to 0 K with Ja data; R5: Ref. [57] extrapolated to 0 K with Barin data; R6: Ref. [60]; R7: Ref. [61], extrapolated to 0 K with Ku data; R8: average of Barin and Ref. [62] extrapolated to 0 K with Barin data.
[b]FM: ferromagnetic; AFM: antiferromagnetic; NM: nonmagnetic; DM: diamagnetic.

FiM initial spin configurations in the primitive cell. When necessary, we also tried searching for a lower-energy GGA+U solution using the U ramping method [76]. After an initial structural relaxation with respect to all internal and external degrees of freedom in the cell, subsequent relaxations had symmetry operations turned off to find lower-energy configurations. Crystal structures are obtained from the Inorganic Crystal Structure Database (ICSD) [77], unless otherwise noted. When the charge of an ion was not explicitly stated in the ICSD listing, we employed a bond-valence sum method [78] to determine the nominal valence of a metal cation using VESTA [79]. For several mixed-valence compounds in case studies, we enumerated possible nominal valence distributions among transition metal atoms in the unit cell, applied LD-U values, and chose the ionic configuration yielding the lowest-energy GGA+U solution. Zero-point energies (ZPEs) are neglected for solids, while ZPEs of molecules are assumed to be included in their chemical potentials fit to simple metal compound formation reactions. We calculated $\Delta\mu_{\text{O}}$ and $\Delta\mu_{\text{F}}$ as 0.689 and 0.433 eV/atom, respectively, by fitting to 0 K formation energies of binary oxides and fluorides of simple metals M = Al, Ba, Sr, Ca, Mg, K, Rb, Na, Li, and Zn with the method described in Refs. [16,35].

B. Selection of the experimental data

We collected ΔH_f^{expt} values mainly from thermochemical tables of JANAF [80] and Kubaschewski [81]. For several compounds, we refer to the thermochemical tables of Barin [82], Wagman and co-workers [83], and other cited literature. For the oxides, ΔH_f^{expt} usually bears relatively small uncertainties compared to fluorides. For most of the fluorides, we carried out a literature survey to acquire more recent ΔH_f^{expt} values, with

uncertainties smaller than the data available in thermochemical tables. We use ΔH_f^{expt} at absolute zero temperature for all compounds (Table I). When a compound has no absolute zero temperature ΔH_f^{expt} reported in thermochemical tables, we extrapolated the 298-K value to 0 K by adding the 0–298 K enthalpy differences to all phases in the formation reaction. For a given compound, the 0–298 K enthalpy difference is obtained by fitting a Debye-type heat capacity to the experimental room-temperature heat capacity ($C_{p,298}$) and entropy (S_{298}) via the procedure outlined by Hautier *et al.* [19], and subsequently integrating the fitted heat capacity from 298 to 0 K. The 0–298 K enthalpy difference of elemental references and diatomic molecules is obtained from JANAF. Using the data reported at 0 K in JANAF tables, we found that our extrapolated ΔH_f^{expt} values are accurate within around 1 meV/atom (see the Supplemental Material [39]). For CoO_2, we employ the enthalpy of formation of $O3 - Li_xCoO_2$ [56] extrapolated to $x = 0$ and accordingly used the O3 structure of CoO_2 rather than the more stable O1 structure. The low-temperature phase of V_6O_{13} is used in formation enthalpy calculations while room-temperature phase is used for the voltage predictions [84]. The only mixed-valence compound we used in U prediction is Co_3O_4 because we could not find the experimental enthalpy for the marginally stable Co^{3+} bearing oxide Co_2O_3. In addition, $BaNi^{4+}O_3$ is the only ternary compound included in our U prediction calculations since we were not able to find reliable enthalpy data for the binary oxide of Ni^{4+}.

IV. RESULTS AND DISCUSSION

A. Local environment dependent U values and energy corrections

The calculated LD-U values and energy corrections for the most common oxidation states of solid oxides and fluorides of M = Ti, V, Cr, Mn, Fe, Co, and Ni are listed in Table II. The details of obtaining these parameters from regular GGA+U total energies and experimental formation enthalpies (Table I) can be found in Appendix B. For all oxides, it is encouraging that the U values in Table II are mostly in a range in agreement with the typical U values used for oxides of these metals (e.g., see Refs. [4,16,19,24,28,36,85]). In our scheme, fluorides turn out to have considerably different $U^X_{M^{a+}}$ values than their corresponding oxides. Therefore, $U^X_{M^{a+}}$ is not well transferable between the ligands O^{2-} and F^- even for metals in the same nominal oxidation state. The U values of oxides vary in a relatively narrow range of approximately 3–6 eV, while for fluorides U values span a wider range. Additionally, our method yields $U^X_{M^{a+}}$ values that increase as the oxidation state $a+$ of M increases in a given M-X system as observed in previous studies [4,28,36,86,87]. Vanadium-oxygen system and MnO_2 are the only exceptions to this trend. In their oxides, V^{2+} and V^{3+} have higher U values than V^{4+} and V^{5+}, and Mn^{4+} has a U smaller than Mn^{3+}. Similar trends were observed before in self-consistent cLDA calculations [4,36]. In fact, Franchini *et al.* [37] pointed out that being closer to the metallic regime, MnO_2 may require a smaller U than other Mn oxides.

While the $U^X_{M^{a+}}$ values are mostly in accord with the typical range of values used in literature, a comparison of the absolute U values is not so meaningful because U strongly depends on the choice of the fitting parameters, or in case of constrained *ab initio* calculations, on the method itself, basis set, projection operators, double-counting term, etc. [24,88]. In fact, the LD-U values provide an acceptable level of accuracy upon predicting the physical properties that they were not fit to (magnetic moments, band gaps, volumes) as shown in Table III, but the primary expectation from these $U^X_{M^{a+}}$ values in Table II is to provide accurate reaction energies in GGA+U

TABLE II. Calculated local environment dependent U values ($U^X_{M^{a+}}$) and total energy corrections ($\Delta\mu^X_{M^{a+}}$) for oxides and fluorides of M = Ti, V, Cr, Mn, Fe, Co, and Ni.

Cation	Ligand	$U^X_{M^{a+}}$ (eV)	$\Delta\mu^X_{M^{a+}}$ (eV/M)	Cation	Ligand	$U^X_{M^{a+}}$ (eV)	$\Delta\mu^X_{M^{a+}}$ (eV/M)
Co^{2+}	O^{2-}	3.75	1.848	Cr^{3+}	O^{2-}	3.04	1.732
Co^{3+}[a]	O^{2-}	4.26	2.116	Cr^{4+}	O^{2-}	3.24	1.871
Co^{4+}	O^{2-}	4.77	2.315	Cr^{6+}	O^{2-}	3.84	2.379
Co^{2+}	F^-	3.05	1.669	Cr^{2+}	F^-	0	0.453
Co^{3+}	F^-	12.04	2.598	Cr^{3+}	F^-	2.82	1.636
				Cr^{4+}	F^-	3.22	1.850
Fe^{2+}	O^{2-}	4.04	1.708				
Fe^{3+}	O^{2-}	4.09	1.730	Mn^{2+}	O^{2-}	2.98	1.457
Fe^{2+}	F^-	0.14	0.686	Mn^{3+}	O^{2-}	4.54	1.844
Fe^{3+}	F^-	4.05	1.700	Mn^{4+}	O^{2-}	3.19	1.331
				Mn^{2+}	F^-	1.40	0.798
Ni^{2+}	O^{2-}	4.40	1.791	Mn^{3+}	F^-	4.69	2.000
Ni^{4+}	O^{2-}	6.07	2.277	Mn^{4+}	F^-	7.31	2.969
Ni^{2+}	F^-	2.85	1.472				
				V^{2+}	O^{2-}	4.90	2.525
Ti^{3+}	O^{2-}	4.35	2.222	V^{3+}	O^{2-}	4.86	2.500
Ti^{4+}	O^{2-}	4.76	2.476	V^{4+}	O^{2-}	3.46	1.738
Ti^{3+}	F^-	2.61	1.457	V^{5+}	O^{2-}	2.97	1.348
Ti^{4+}	F^-	9.11	4.503	V^{3+}	F^-	5.24	2.685
				V^{4+}	F^-	6.67	3.354

[a]Due to lack of thermochemical data for a binary Co^{3+} oxide, we calculated this value for Co^{3+} using Co_3O_4.

TABLE III. Magnetic moments (m), band gaps (E_g), and volumes of binary 3d-metal oxides and fluorides calculated using the LD-U values (Table II). Experimental data are given in brackets. Despite their parametrization using thermochemical data only, LD-U values provide a reasonable accuracy in m and E_g for most of the compounds, and typically overestimate volume as observed in previous GGA+U calculations [18].

Compound	m (μ_B)	E_g (eV)	Volume (Å^3/atom)[a]
CoO	2.67 (3.35) [89]	2.43 (2.4–2.5) [20,90]	9.90 (9.65)
Co_3O_4[b]	2.69, 0 (3.02, 0) [64]	2.07 (1.6) [90]	9.69 (9.37)
	2.66, 0	1.97	9.70
CoO_2(O1)	1.36	0[c] (0) [91]	10.83 (9.87) [92]
CoO_2(O3)	1.36	1.02	11.14
CoF_2	2.77 (2.57) [93]	2.87	12.10 (11.68)
CoF_3	3.99 (4.4) [66]	4.72	11.53 (12.10)
Cr_2O_3	2.97 (2.76) [67]	2.54 (2.8) [94]	10.18 (9.66)
CrO_2	2.50 (2.0) [95]	0[d] (0) [96]	9.95 (9.48)
CrO_3	0	2.07	16.82 (14.71)
CrF_2	3.74 (3.6) [69]	0.66	13.56 (12.96)
CrF_3	2.95 (3) [66]	2.17	12.53 (11.87)
CrF_4	2.08	1.59	14.22 (12.86)
FeO	3.69 (3.32) [63]	1.51 (2.4) [97]	10.53 (9.96)
Fe_2O_3	4.16 (4.9) [98]	2.19 (2.0–2.7) [97]	10.31 (10.09)
Fe_3O_4	4.074, 3.674, 4.180[e] (4) [74]	0.75 (0.07-0.25) [74,99]	10.97 (10.58)
FeF_2	3.62 (4.05) [100]	0.56	12.50 (12.16)
FeF_3	4.36 (5) [66]	3.87	13.48 (12.98)
MnO	4.54 (4.58) [101]	1.59 (1.84–2.60) [102]	11.23 (11.24)
Mn_2O_3	3.95 (3.4–3.9) [71]	0.73	11.00 (10.44)
MnO_2	2.95 (2.40) [103]	0.08 (0.28–0.7) [102]	9.65 (9.26)
MnF_2	4.60 (5.12) [100]	2.76 (9.9–10.2) [102]	13.55 (13.10)
MnF_3	3.92 (4) [66]	0.67	14.20 (12.55)
MnF_4	3.45 (3.85) [104]	0.98	12.96 (12.06)
NiO	1.65 (1.90) [101]	2.64 (3.7–4) [102]	9.27 (9.12)
NiF_2	1.75 (1.99) [100]	3.10	11.50 (11.11)
Ti_2O_3	0.95	1.53 (0.02–0.05) [102]	11.63 (10.49)
TiO_2	0	2.28 (3.0–3.75) [102]	11.08 (10.41)
TiF_3	0.94	0.66	15.34 (14.54)
TiF_4	0	4.79	15.31 (14.00)
VO	2.72	2.45	10.95 (8.74)
V_2O_3	1.91	2.42 (0.2-1.51) [94,97]	10.94 (10.00)
VO_2	1.08	0.88 (0.8) [74]	10.35 (9.86)
V_2O_5	0	2.13 (2–2.54) [97,102]	13.82 (12.80)
VF_3	1.93 (2) [66]	2.90	13.84 (12.93)
VF_4	1.06	4.08	14.13 (12.83)

[a]Experimental volumes are taken from the corresponding ICSD entries listed in Table I.
[b]First row: calculated using the constant U of 4.26 eV. Second row: calculated using the LD-U values for Co^{2+} and Co^{3+}. Moments are given in the order Co^{2+} and Co^{3+}.
[c]Semimetal.
[d]Half-metal, in agreement with experiments [96].
[e]First moment: 8a Fe site. Following two moments: 16b site.

thermochemistry. These U values should only be considered as thermochemical corrections to the total energy, and may not give accurate results for any other property calculated with GGA+U. In the following sections, we present a detailed analysis of the performance of the LD-GGA+U parameters in GGA+U thermochemistry.

B. Transferability of LD-GGA+U parameters: Ternary oxide formation enthalpies

The accuracy of the conventional constant-U GGA+U thermochemistry together with energy corrections has already been well tested [19,38,43]. The $U^X_{M^{a+}}$ values we calculate in this work, on the other hand, are not constant for a given M, but explicitly dependent on its local environment in the compound defined by $a+$ and X. We expect this local environment dependence to provide an improvement in thermochemical accuracy over the constant-U methods when the calculated LD-U values are used in calculations of new compounds (i.e., compounds not in the fit set in Table I). Accordingly, we test the transferability of the determined LD-GGA+U parameters by comparing the calculated formation enthalpies of a wide variety of metal oxides to the experimental values. This test set includes 52 3d-metal bearing oxides such as regular transition

metal ternary (e.g., $CaCr_2O_4$), mixed transition metal ternary (e.g., $MnFe_2O_4$), and mixed-valence binary (e.g., Fe_3O_4) oxides (see Table IV for the entire list). For this test set, the LD GGA+U framework gives a remarkably small mean absolute error (MAE) of 19 meV/atom with respect to the absolute zero-temperature experimental formation enthalpies. Since the oxides in the test set were not used while training the $U^X_{M^{a+}}$ values, such a small MAE validates the excellent transferability of LD-GGA+U parameters, and proves that LD-GGA+U provides highly accurate thermochemistry. In fact, the average reported uncertainty of the experimental formation enthalpies of the compounds in the current test set is ∼10 meV/atom, which means the predictive power of the LD-GGA+U scheme with a MAE of 19 meV/atom is very close to the experimental chemical accuracy.

The very high accuracy of LD-GGA+U cannot be attributed solely to the use of LD-U values. LD-GGA+U framework is a combination of various methods added over regular GGA to correct its deficiencies in thermochemistry of transition metal compounds. These corrections include (i) a separate fitting of chemical potentials of diatomic molecules, (ii) replacing GGA with GGA+U functional to correct the overdelocalization of electrons, (iii) using LD-U values to improve the thermochemical accuracy in those GGA+U calculations, and finally (iv) using the corresponding total energy corrections to ensure energetic compatibility among all LD-GGA+U calculations. Therefore, to investigate the contribution of using LD-U values and energy corrections on the thermochemical accuracy, we devise intermediate schemes between GGA and LD-GGA+U that incorporate different levels of corrections as shown in Figs. 2 and 3. The correction schemes we test are as follows:

(i) GGA [fit:O]: Only the O_2 chemical potential is corrected. All schemes listed below also include the same O_2 chemical potential correction.

(ii) GGA [fit:M,O]: LD energy corrections are derived (at $U = 0$) and used for M.

(iii) GGA+U [S1]: Jain *et al.*'s average energy correction factors [38] with constant-U values given therein are used for M.

(iv) GGA+U [S2]: Same as S1, except the average energy correction factors are recalculated using the data in this work.

(v) GGA+U [S3]: Constant U of S1, with corresponding LD energy corrections calculated in this work.

(vi) LD-GGA+U: LD-U values and energy corrections (current method).

For methods S1, S2, and S3, we determined a constant-U value for Ti with the method of Wang *et al.* [16] as 4.4 eV with an average energy correction of 2.244 eV/atom in this work because Ti was not available in Refs. [16,38]. Using plain GGA+U for both M and $MX_{a/x}$ leads to a very large MAE [38], thus we do not repeat such calculations here.

Correcting GGA formation enthalpies with $\Delta\mu_O$ given in Sec. III (i.e., introducing the scheme GGA [fit:O] in Fig. 2) obviously corrects the systematic underestimation of formation enthalpies, and the GGA MAE of 330 meV/atom drops to 165 meV/atom for our test set. This error, however, is still an order of magnitude larger than the average experimental uncertainty of ∼10 meV/atom in this set of compounds. It is also important to reveal how MAE changes if we still use plain GGA ($U = 0$) for all phases in the formation reaction [Eq. (4)], but further add a corresponding valence and ligand (i.e., local environment) dependent correction for M. These corrections can be readily obtained at $U = 0$ from Fig. 8. Correcting GGA this way (the GGA [fit:M,O] scheme in Fig. 2) improves the enthalpy predictions compared to the GGA [fit:O] scheme, and substantially lowers the MAE as shown in Fig. 3. Thus, a portion of the error associated with representations of M and $MX_{a/x}$ in GGA can be systematically corrected with LD energy correction factors, even without a +U calculation. Although it is hard to quantify how much of the remaining error overlaps with correlation effects, it is clear that a further improvement requires GGA+U to more accurately describe the electronic structure of these materials.

For the next scheme (labeled as S1 in Fig. 3), we use the GGA/GGA+U mixing method by Jain *et al.* [38] summarized in Sec. II B. With this method, the MAE drops to ∼31 (34) meV/atom with respect to 0 K (298 K) formation enthalpies, with the constant-U values and average energy corrections reported by Jain *et al.* [38] (except for Ti as noted before). If we recalculate the average corrections with the experimental data utilized in this work (i.e., for all oxides of a given M, read the corrections from Fig. 8 at the U value listed by Jain *et al.*, and calculate their average), the MAE drops considerably (labeled as S2 in Fig. 3). Obviously, any improvement in MAE over this scheme will be small and depend strongly on the temperature effects as well.

The difference between S2 and the current LD-GGA+U method in Fig. 3 is using a constant U and a constant (averaged) energy correction for a given M in the former method, and using their local environment dependent counterparts in the latter method. Thus, it is still not clear at this point whether the LD energy corrections or the LD-U values are actually responsible for the further improvement provided by LD-GGA+U. To test this, we devise the intermediate scheme (S3) between S2 and LD-GGA+U. In the S3 scheme, we still use the constant-U values from Jain *et al.* [38] but, instead of the average corrections, we use LD energy corrections corresponding to these constant-U values. In other words, unlike the S2 scheme, energy corrections read from Fig. 8 are not averaged but directly used as LD energy corrections in the S3 scheme. We find that the MAE of S3 is between S2 and LD-GGA+U in Fig. 3. Actually, the improvement S3 provides over S2 with respect to 298-K data is not as good as that it provides over 0-K data. Since the only difference between S3 and LD-GGA+U schemes is the use of LD-U values in the latter scheme, we conclude that the associated drop of MAE when we switch from S3 to LD-GGA+U is solely related with the use of the predicted LD-U values. This demonstrates that the LD-U values provide an improvement in the thermochemical description of the compounds via GGA+U, beyond what would be achieved via using a constant U for all oxidation states of a 3d metal.

The LD-U values and corresponding energy corrections are calculated in the chemical space of M = Ti, V, Cr, Mn, Fe, Co, and Ni and X = O and F. We expect the transferability of these parameters to a chemical space with other ligands to be limited. For example, when the ligand is changed to SiO_4^{4-}, we observed that the present $U^O_{M^{a+}}$ and $\Delta\mu^O_{M^{a+}}$ values result in larger errors around 50 meV/atom on average (see

TABLE IV. Enthalpies of formation of 52 3d-metal oxides (and 6 silicates) calculated by GGA (with fitted O_2 chemical potential) and LD-GGA+U, as well as the corresponding experimental values. Experimental values are either at absolute 0 K or extrapolated to absolute 0 K using reported $C_{p,298}$ and S^0_{298}, unless otherwise noted. Source of experimental enthalpy data and ICSD No. of compound crystal structure are also listed. Enthalpies are in units of eV/atom.

Compound	GGA	LD-GGA+U	Experiment	Expt. Ref.[a]	ICSD No.
Mixed					
$CoCr_2O_4$	−1.974	−2.095	−2.111	e-Ku	27507
$CoFe_2O_4$	−1.416	−1.600	−1.605	e-Ku	166200
$CoTiO_3$	−2.522	−2.460	−2.494	e-Ku	16548
Fe_2TiO_4	−2.244	−2.231	−2.219	e-Ku	18186
Fe_3O_4	−1.686	−1.656	−1.650	Ja	85806
$FeCr_2O_4$	−2.047	−2.141	−2.136	e-Ku	43269
$FeTiO_3$	−2.662	−2.537	−2.558	e-Ku	9805
Mn_2TiO_4	−2.514	−2.573	−2.587	e-Ku	22313
$MnFe_2O_4$	−1.619	−1.839	−1.813	e-Ku	24497
$MnTiO_3$	−2.857	−2.793	−2.807	e-Ku	44407
MnV_2O_6	−2.624	−2.310	−2.303	Wa298	40850
$NiCr_2O_4$	−1.999	−2.006	−2.028	e-Ku	280061
$NiFe_2O_4$	−1.530	−1.548	−1.587	Wa	52387
$NiTiO_3$	−2.505	−2.430	−2.478	e-Ku	38157
V_3O_5	−2.762	−2.515	−2.504	Wa298	16445
V_6O_{13}-lt	−2.821	−2.412	−2.414	R1	281620
Ti oxides					
Al_2TiO_5	−3.470	−3.343	−3.360	e-Ku	27681
Ba_2TiO_4	−3.426	−3.231	−3.302	e-Ku	2625
$BaTiO_3$	−3.528	−3.343	−3.404	e-Ku	100463
$Ca_4Ti_3O_{10}$	−3.559	−3.405	−3.446	e-Ku	86242
$CaTiO_3$	−3.590	−3.420	−3.430	e-Ku	62149
Li_2TiO_3	−3.017	−2.860	−2.869	e-Ku	15150
$MgTi_2O_5$	−3.477	−3.240	−3.234	Wa	37232
$MgTiO_3$	−3.416	−3.223	−3.241	e-Ku	65794
$Na_2Ti_3O_7$	−3.207	−2.943	−2.993	e-Ku	250000
Sr_2TiO_4	−3.476	−3.342	−3.366	R2	20293
$SrTiO_3$	−3.592	−3.405	−3.416	R2	80873
Zn_2TiO_4	−2.524	−2.404	−2.432	e-Ku	109093
V oxides					
$Ca_2V_2O_7$	−3.234	−2.920	−2.892	e-Ku	20609
CaV_2O_6	−3.076	−2.699	−2.669	e-Ku	21064
$Mg_2V_2O_7$	−3.006	−2.691	−2.660	e-Ku	2321
MgV_2O_6	−2.905	−2.523	−2.523	e-Ku	10391
$Na_4V_2O_7$	−2.620	−2.329	−2.322	e-Ku	35635
$NaVO_3$	−2.721	−2.379	−2.372	R3	29450
Cr oxides					
$CaCr_2O_4$	−2.390	−2.685	−2.698	e-Ku	6131
Cs_2CrO_4	−1.997	−2.092	−2.110	e-Ku	30204
K_2CrO_4	−2.401	−2.076	−2.071	R4	30266
$MgCr_2O_4$	−2.607	−2.618	−2.627	e-Ku	52386
$MgCrO_4$	−2.583	−2.202	−2.177	R4	18120
Na_2CrO_4	−2.323	−1.999	−1.980	R5	26330
$NaCrO_2$	−2.090	−2.246	−2.260	e-Ku	24595
$ZnCr_2O_4$	−2.247	−2.254	−2.279	e-Ku	24495
Mn oxides					
Mn_2SiO_4	−2.370	−2.592	−2.559	e-Ku	26376
$MnAl_2O_4$	−2.975	−3.060	−3.093	e-Ku	157282
Fe oxides					
$Ca_2Fe_2O_5$	−2.434	−2.420	−2.449	e-Ku	15059
$CaFe_2O_4$	−2.099	−2.166	−2.182	e-Ku	16695
$CaFeSi_2O_6$	−2.943	−3.012	−2.939	R6	10227
Fe_2MgO_4	−1.995	−2.095	−2.102	e-Wa	24493

TABLE IV. (*Continued*.)

Compound	GGA	LD-GGA+U	Experiment	Expt. Ref.[a]	ICSD No.
Fe_2SiO_4	−2.068	−2.268	−2.186	Wa	34817
$FeAl_2O_4$	−2.808	−2.894	−2.897	e-Ku	56117
$FeSiO_3$	−2.449	−2.561	−2.491	Wa	34863
$LiFeO_2$	−1.506	−1.939	−1.958	R7	51767
$NaFeO_2$	−1.717	−1.794	−1.800	e-Ku	37157
$ZnFe_2O_4$	−1.634	−1.730	−1.736	e-Ku	24496
Co oxide					
Co_2SiO_4	−1.901	−2.134	−2.082	e-Ba	200705
$CoAl_2O_4$	−2.755	−2.869	−2.879	e-Ku	21116
Ni oxide					
Ni_2SiO_4	−1.892	−2.089	−2.062	e-Ku	40992
$NiAl_2O_4$	−2.720	−2.817	−2.820	Wa	608815

[a]Ja: Janaf [80] at 0 K; e-Ku: Kubaschewski [81] extrapolated to 0 K; Wa: Wagman *et al.* [83] at 0 K; Wa298: Wagman *et al.* at 298 K; e-Ba: Barin [82] extrapolated to 0 K; R1: Ref. [126]; R2: Ref. [127]; R3: Ref. [128]; R4: Ref. [129]; R5: Ref. [129] extrapolated to 0 K with Ku; R6: Ref. [130] extrapolated to 0 K with data therein; R7: average of Wa and Ku, extrapolated to 0 K with Ku.

Table IV). Including the silicates in the test set increases the MAE to 23 meV/atom. Therefore, $U^{O}_{M^{a+}}$ and $\Delta\mu^{O}_{M^{a+}}$ are clearly not very well transferable to systems with $X = SiO_4^{4-}$. Moreover, applying LD-GGA+U to mixed-ligand compounds (e.g., oxyfluorides) may not be straightforward. In principle, new LD-GGA+U parameters should be calculated for the mixed-ligand compounds using the corresponding experimental thermochemical data, but such thermochemical data are very scarce. As a practical alternative, we recommend using $\bar{U}$ of the reaction between the compounds of the distinct ligands, for mixed-ligand coordinated M. For example, $\bar{U}$ of the reaction $Fe_2O_3 + 3F_2 \rightarrow 2FeF_3 + 1.5O_2$ can be used for FeOF. As a final remark, we should note that the LD-GGA+U framework does not restrict the use of additional local environment descriptors such as bond lengths or geometry of the M-X coordination. However, we expect such features to be more important in transition metal complexes [105] and not to vary considerably in crystalline solids. The excellent transferability of LD-U parameters validates that a and X are sufficient to describe the local environment of M.

An alternative method for improving the accuracy of thermochemical predictions of transition metal oxide reaction energies is using computationally demanding hybrid functionals such as HSE06 [106,107], which do not require a parameter like U as an input. Recently, Chevrier *et al.* [18] showed that HSE06 yields an average error of 0.35 eV per O_2 for the formation energies of transition metal oxides. This error is an order of magnitude larger than what is typically achieved using the LD-GGA+U method (see Table IV). As an illustrative example, the LD-GGA+U method yields the formation enthalpy of Fe_3O_4 within a few meV of the experimental value (Table IV), whereas the corresponding HSE06 error is on the order of 0.2 eV/atom [18]. Therefore, while HSE06 is not likely to provide a significant accuracy gain in reaction energies at the expense of its higher cost of computation compared to the LD-GGA+U method (or other schemes that allow mixing GGA and GGA+U functionals [38,43]), further

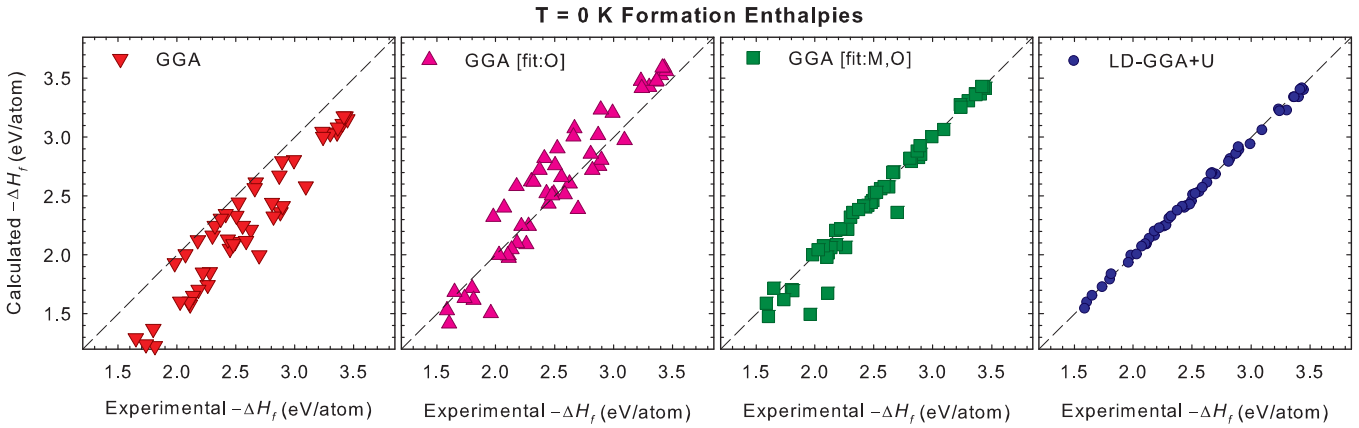

FIG. 2. (Color online) Enthalpy of formation of 52 3d-metal oxides calculated by GGA, GGA with O_2 correction (GGA [fit:O]), GGA with O_2 correction and LD energy corrections for M (GGA [fit:M,O]), and local environment dependent GGA+U (LD-GGA+U), compared to the experimental enthalpy of formation extrapolated down to absolute zero. Dashed lines represent perfect agreement between the calculated and experimental values.

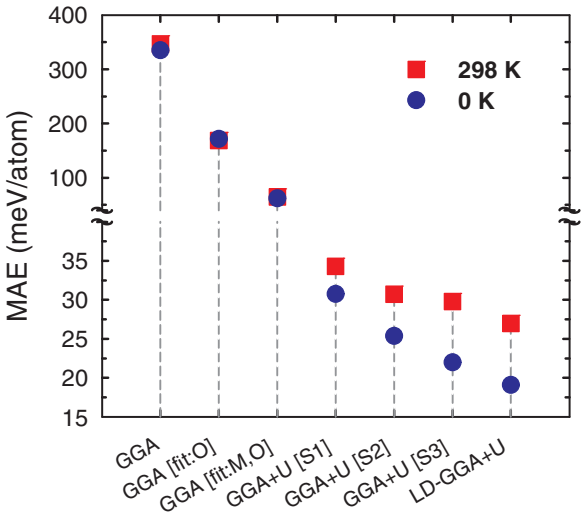

FIG. 3. (Color online) Mean absolute error (MAE) of formation enthalpies of 52 ternary oxides calculated by GGA and GGA+U with various parametrizations and correction schemes. GGA [fit:O] and GGA [fit:M,O] include O_2 correction, and O_2 and LD energy correction for M, respectively. In S1, S2, and S3, we employ the U values used in Ref. [38]. In S1, the average energy corrections for M are also taken from Ref. [38]. In S2, we recalculate the average corrections with the data in this work. In S3, we calculate LD energy corrections for M, corresponding to the constant U used. All correction schemes include the O_2 correction.

exploration and comparison of hybrid functionals with the current approach would be of considerable interest.

C. Applications of the LD-GGA+U method

Following the accurate prediction of formation enthalpies, we further test the performance of the LD-GGA+U method in more complex redox processes, such as in lithium-ion battery voltages and stabilities of mixed-valence compounds in this section.

1. Li_xCoO_2 system

In this first example, we calculate the voltage of the well-known Li-ion battery cathode $LiCoO_2$ with the conventional constant-U GGA+U and the new LD-GGA+U methods. For the lithiation of a cathode host Li_{x_1}Host via the reaction $Li_{x_1}\text{Host} + (x_2 - x_1)\text{Li} \rightarrow Li_{x_2}\text{Host}$, the average lithiation voltage with respect to a Li anode can be calculated as [1,109]

$$\langle V\rangle(x_1,x_2) = -\frac{E[Li_{x_2}\text{Host}] - E[Li_{x_1}\text{Host}] - (x_2 - x_1)E[\text{Li}]}{(x_2 - x_1)e}. \quad (10)$$

The average voltage corresponding to complete lithiation of CoO_2, i.e., $\langle V\rangle(0,1)$, as a function of U with the constant-U GGA+U approach (where the same U is applied on the d manifold of Co in both $LiCoO_2$ and CoO_2) is shown in Fig. 4(a). The voltage $\langle V\rangle(0,1)$ given by the constant-U GGA+U with the low-spin (LS) t_{2g}^6 configuration for Co^{3+} follows a concave-down parabolic trend. The maximum constant-U voltage is around 3.84 V at a U of ~5.2 eV (in agreement with Chevrier *et al.* [18]), which is lower than the experimental measurements. The high-spin (HS) $t_{2g}^4 e_g^2$ configuration for Co^{3+} becomes stable above $U \sim 5.3$ eV. At large U, this HS-Co^{3+} can reproduce the experimental voltage. However, such a solution is unphysical since Co^{3+} in $LiCoO_2$ is known to adopt a LS configuration [110]. On the contrary, the LD-GGA+U calculation, where Co^{3+} is treated with a U of 4.26 eV (i.e., preserving the stability of LS-Co^{3+} over HS) and Co^{4+} is treated with a U of 4.77 eV, yields a value closer to the experimental $\langle V\rangle(0,1)$ compared to the constant-U GGA+U.

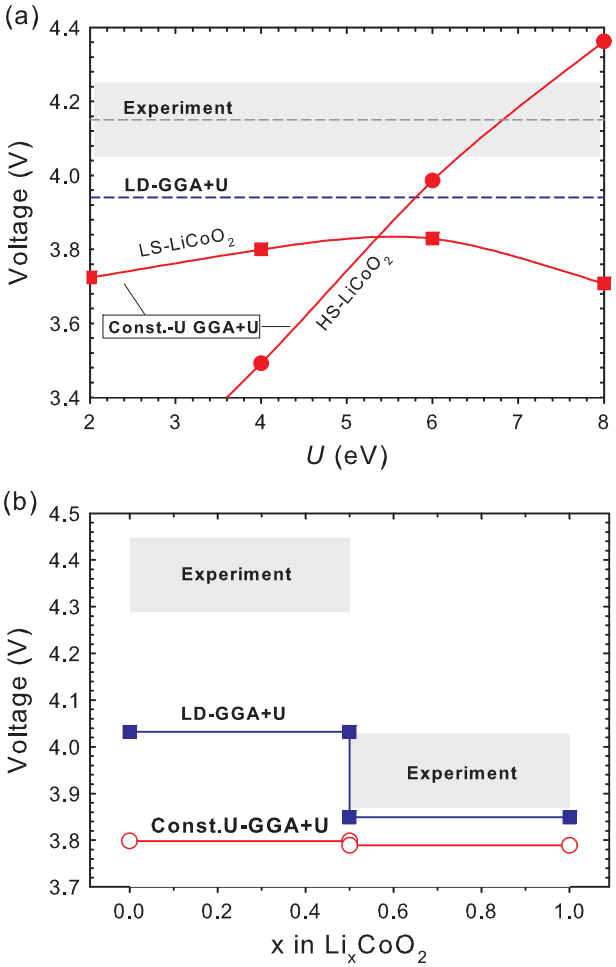

FIG. 4. (Color online) Average constant-U GGA+U voltage calculated as a function of U, average LD-GGA+U voltage, and the corresponding experimental voltage of complete (de)lithiation of Li_xCoO_2 [$\langle V\rangle(0,1)$] are given in (a). The LD-GGA+U voltage and constant-U GGA+U voltages of Li_xCoO_2 in regions $x = 0$–0.5 and 0.5–1.0 are compared to the average experimental voltages in the corresponding regions in (b). Experimental voltages are shown as shaded areas that are bound by average charge and average discharge voltages in corresponding regions given in Ref. [108].

The lithiation path of $LiCoO_2$ involves multiple mixed-valence compounds [111], one of which is the experimentally confirmed monoclinic phase $Li_{0.5}CoO_2$ [112]. As shown in Fig. 4(b), including this compound divides the average $\langle V\rangle - x$ profile into two subregions, with respective voltages $\langle V\rangle(0,0.5)$ and $\langle V\rangle(0.5,1)$. LD U provides an improvement over constant U upon predicting both $\langle V\rangle(0,0.5)$

and $\langle V\rangle(0.5,1)$. More importantly, a significant voltage step with a size of $\Delta V = \langle V\rangle(0,0.5) - \langle V\rangle(0.5,1)$ appears at $x = 0.5$ in the voltage profile. Using Eq. (10), we can show that $\Delta V = -4\Delta E/e$, where ΔE is

$$\Delta E = E\left[\mathrm{Li}_{0.5}\left(\mathrm{Co}^{3+}_{0.5}\mathrm{Co}^{4+}_{0.5}\right)\mathrm{O}_2\right] - \tfrac{1}{2}E[\mathrm{LiCo}^{3+}\mathrm{O}_2] - \tfrac{1}{2}E[\mathrm{Co}^{4+}\mathrm{O}_2]. \quad (11)$$

It is clear that ΔE is the energy of formation of $Li_{0.5}CoO_2$ from the end members CoO_2 and $LiCoO_2$ as in the reaction $\frac{1}{2}Co^{4+}O_2 + \frac{1}{2}LiCo^{3+}O_2 \rightarrow Li_{0.5}(Co^{3+}_{0.5}Co^{4+}_{0.5})O_2$. Hence, ΔV is a measure of the stability of $Li_{0.5}CoO_2$. We find that $Li_{0.5}CoO_2$ becomes unstable (i.e., $\Delta V < 0$ or $\Delta E > 0$) for $U >\sim 3.4$ eV in constant-U GGA+U. Thus, a U around 5.2 eV that gives the maximum constant-U voltage $\langle V\rangle(0,1)$ of 3.84 V cannot even qualitatively reproduce the experimental voltage step at $x = 0.5$. If we employ a constant U of 3.3 eV [16], $Li_{0.5}CoO_2$ becomes marginally stabilized as is evident from the very small ΔV that appears in the constant-U profile in Fig. 4(b). *Therefore, a single-U value cannot adequately describe the physics underlying the phase stability and voltages in the* Li_xCoO_2 *system.* In contrast, the magnitude of ΔV is much more accurately captured with LD-GGA+U. We should emphasize that ΔV is independent of the energy corrections in LD-GGA+U, since they cancel out in Eq. (11). Hence, the improvement in ΔV with LD-GGA+U can be solely attributed to the use of unique LD-U values for Co^{3+} and Co^{4+}. This case study shows that the limitations of using a constant U for all oxidation states of a metal such as Co in processes similar to Eq. (11) can be effectively overcome using the current LD-GGA+U parameters.

2. $Li_xV_6O_{13}$ system

An intricate lithiation process takes place in the $Li_xV_6O_{13}$ cathode, where voltage steps in the region $x = 0$–3 are very small as shown in Fig. 5. The room-temperature polymorph of the starting cathode V_6O_{13} has a $C2/m$ space group with

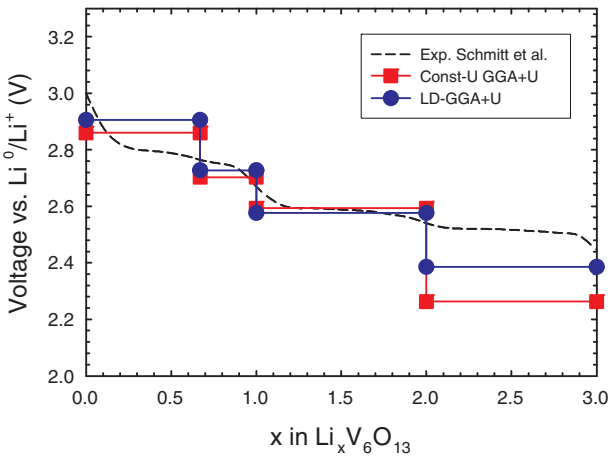

FIG. 5. (Color online) Lithiation voltage of mixed-valence $Li_xV_6O_{13}$ between $x = 0$ and 3 calculated by the constant-U GGA+U and the current LD-GGA+U methods, compared to the experimental discharge profile extracted from the paper by Schmitt *et al.* [113]. Constant-U calculations are done with $U = 3.1$ eV reported by Wang *et al.* [16] for V.

two V^{5+} and four V^{4+} ions per formula unit. Upon lithiation of V_6O_{13}, reduction proceeds as $V^{5+} \rightarrow V^{4+} \rightarrow V^{3+}$ in multiple steps via a series of two-phase reactions. Lithium first enters between the single and double octahedra layers of V_6O_{13}, accompanied by distortion of the crystal and V-O bonds, and charge ordering [113,114]. In LD-GGA+U calculations, stabilities of the intermediate compounds producing voltage steps such as in Fig. 5 may or may not depend on the energy correction factors. When the reaction involves two adjacent oxidation states [e.g., as in describing the stability of $Li_{0.5}CoO_2$ relative to end members in Fig. 4(b)], correction factors cancel out and step size (i.e., stability) is determined only by the LD-U values. On the other hand, when the reaction spans three oxidation states (as in describing the stability of intermediate phases in the $Li_xV_6O_{13}$ system in the range $0 < x < 3$ relative to the end members), the LD energy corrections do not cancel out, and stabilities depend critically on the energy compatibility established by such corrections. Therefore, predicting the phase equilibria in the $Li_xV_6O_{13}$ system is a stringent test for the LD-GGA+U method.

We compare the lithiation profiles of $Li_xV_6O_{13}$ calculated using the constant-U and LD-GGA+U methods together with Eq. (10) to the experimental profile in Fig. 5. Constant-U and LD-GGA+U methods both produce similar results up to $x = 2$ (i.e., up to reduction of all V^{5+} to V^{4+}), in good agreement with the experimental profile [113]. The agreement of both methods with the experiment in this region implies that V^{4+} and V^{5+} require U values close enough such that they can be treated accurately with the same constant-U value. Further lithiation up to $x = 3$ proceeds via reduction of V^{4+} to V^{3+}. In this region, both methods underestimate the voltage, but the LD-GGA+U calculation is significantly closer to the experimental plateau compared to the constant-U calculation. The compounds with $x = 0.67$, 1, and 2 are ordered, while for $x = 3$, one of the Li sites in the structure reported by Höwing *et al.* [115] is noncentrosymmetric with equivalent probabilities for occupation slightly above and below the centrosymmetric site on the single layer. Thus, the slight discrepancy in $\langle V\rangle(2,3)$ might be a result of the $x = 3$ structure being not represented well in our fully ordered DFT calculations. In short, Fig. 5 shows that the LD-U values and energy corrections not only preserve the phase stabilities observed in the experiment and reproduced by conventional GGA+U along $V^{5+} \rightarrow V^{4+} \rightarrow V^{3+}$, but also provide an improved estimation for $\langle V\rangle(2,3)$ compared to the conventional GGA+U.

3. Li_xFeF_3 system

As a potential high-capacity fluoride cathode for Li-ion batteries, FeF_3 has been subject to multiple experimental [117–121] and computational studies [38,43,116] and is an important system to test the performance of LD-GGA+U in 3d-metal fluorides. Lithiation of FeF_3 proceeds in two major steps corresponding to Fe^{3+}/Fe^{2+} and Fe^{2+}/Fe redox couples [118]. Each step involves intricate subreactions that proceed along with competition among kinetically faster Li insertion into the present phases and sluggish conversion reactions requiring nucleation of new phases [116,119]. Lithiation starts with a conversion reaction producing the (tri)rutile $Li_{0.5}FeF_3$

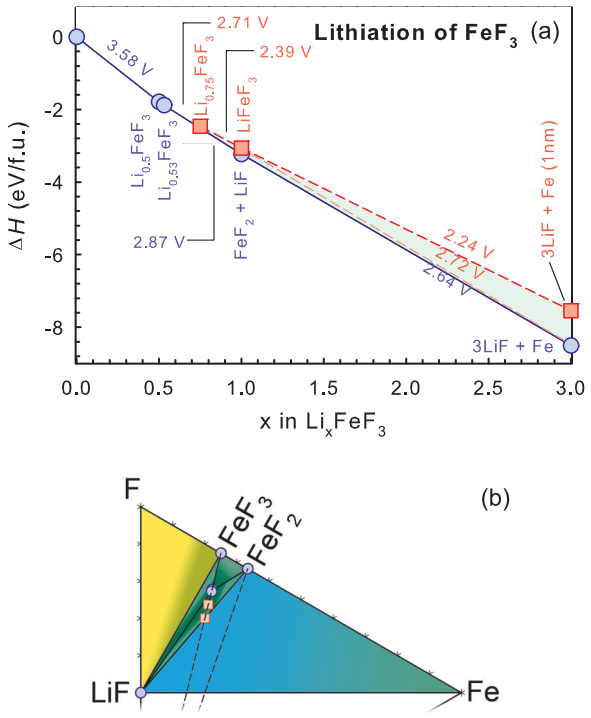

FIG. 6. (Color online) (a) Enthalpy of formation of phases (or phase mixtures) from FeF_3 and Li metal as in the reaction $FeF_3 + xLi \rightarrow Li_xFeF_3$ along the $FeF_3 - Li$ cross section of the Li- Fe-F ternary convex hull calculated with LD-GGA+U. Li_xFeF_3 denotes the composition at a Li content of x, and the corresponding ground state can be mixture of phases as in $FeF_2 + LiF$ at $x = 1$. Circles and solid lines connecting them represent the stable phases and the convex hull (equilibrium lithiation path), respectively. Squares and dashed lines represent unstable phases and possible nonequilibrium paths, respectively. Lithiation voltages (negative of the slope of the lines) in distinct phase regions along equilibrium and nonequilibrium paths are marked on the plot. For the Fe phase labeled as Fe (1 nm), we added the surface energy of the ∼1 nm Fe particle reported in Ref. [116] to the GGA energy of bulk Fe. The LiF-Fe-F region of the calculated ground-state ternary phase diagram is given in (b), where dashed lines point towards the Li corner. Phase regions in (b) are colored to differentiate the regions, merely as a guide to the eye.

phase and continues with insertion of Li up to $x \approx 1.0$ [120]. Further reduction occurs via conversion of the lithium inserted phase ($LiFeF_3$) [38] to LiF and Fe as $LiFe^{2+}F_3 + 2Li \rightarrow 3LiF + Fe$. For this reaction, we calculate the voltage as 2.72 V with LD-GGA+U in agreement with experiments [118,119] and previous GGA/GGA+U calculations [38,43,116].

As shown in Fig. 6(a), we find that $LiFeF_3$ is, in fact, slightly unstable against decomposition to LiF and FeF_2, and it is 33 meV/atom above the convex hull. The predicted thermodynamic stability of the phase mixture $LiF + FeF_2$ at $x = 1.0$ is actually supported by the lithiation mechanism of FeF_2 batteries. Any stable phase on the $LiF - FeF_2$ tie-line in Fig. 6(b) would divide the $LiF - FeF_2 - Fe$ stability region into multiple regions, and subsequently lead to a two-step lithiation process for FeF_2. However, this contradicts the experiments where lithiation of FeF_2 occurs essentially via a single-step conversion reaction starting with FeF_2 and yielding LiF and Fe [122]. Therefore, the Li-Fe-F ground-state stability map predicted by LD-GGA+U [Fig. 6(b)] agrees well with the experiments.

To further analyze the stability of lithium inserted $Li_{0.5}FeF_3$ structures up to $LiFeF_3$, we test two additional intermediate structures: $Li_{\sim 0.53}FeF_3$ (one Li atom inserted into a $2 \times 2 \times 2$ supercell of 18-atom $Li_{0.5}FeF_3$ unit cells) and $Li_{0.75}FeF_3$ (one Li atom inserted into a single 18-atom $Li_{0.5}FeF_3$ unit cell) where Li insertion sites are determined by a preliminary electrostatic energy minimization. We find that the $x \approx 0.53$ configuration is barely on the convex hull, and the $x \approx 0.75$ one is above it by only 9 meV/atom. Therefore, as more Li is inserted, the insertion phase starts to rise more above the convex hull (i.e., becomes thermodynamically unstable), reaching 33 meV/atom above the hull at $x = 1.0$. This instability, however, is marginal, and kinetically favorable insertion mechanisms can dominate as observed in experiments [120]. Decomposition of the unstable single phase Li_xFeF_3 to LiF and FeF_2 is likely to be kinetically hindered as it requires mass transport. Further reduction beyond $x \approx 1.0$ proceeds via conversion, yielding mainly nanosized Fe domains in a LiF matrix [118,120]. Doe *et al.* [116] showed that the small size of Fe particles can influence the voltage in this region. If we incorporate the energy difference between a ∼1 nm Fe nanoparticle and bulk Fe from their study, an alternative lithiation path emerges in Fig. 6(a). We observe that the calculated voltage gets closer to the experimental discharge plateau of around 2 V in the range $x = 1.0$–3.0 [118–120] along this alternative metastable path. We conclude that the intricate phase stability is well accounted for with LD-GGA+U in the Li-Fe-F system.

4. $V_{1.5}O_{1+x}$ system

Phase stability in the vanadium-oxygen system is quite complex due to presence of the mixed-valence V_nO_{2n-1} phases (V_3O_5 and Magnéli phases with a positive integer $n \geqslant 4$) between V_2O_3 and VO_2, and mixed-valence V_3O_7 and V_6O_{13} phases between VO_2 and V_2O_5 [123,124]. In Fig. 7, we show that the mixed-valence phases with known low-temperature structures [125] acquired from the ICSD are predicted to be on the convex hull (or very close to the hull) using the LD-GGA+U method, in agreement with the stable phases in the available experimental phase diagram [123]. Only V_5O_9 and V_7O_{13} are slightly above the hull, but the distance between their formation energies and the convex hull are 5 and 7 meV/atom, respectively, which are on the order of the typical experimental thermochemical accuracy (see Sec. IV B). The constant-U method finds two of the six mixed-valence compounds we considered to be substantially above the hull (i.e., unstable). Moreover, constant-U GGA+U formation enthalpy of VO_2 with respect to the end members is approximately 30% more negative compared to the experimental value, where LD-GGA+U is exact by construction (V_2O_3, VO_2, and V_2O_5 were already in our LD-GGA+U fitting set). It is important to note that to improve the constant-U calculations, we tried fitting a U value other than 3.1 eV with the method of Wang *et al.* [16] to the experimental enthalpy of the reaction $V_2O_3 + V_2O_5 \rightarrow 4VO_2$. However, the constant-$U$ GGA+U enthalpy of this reaction shows a concave-down parabolic

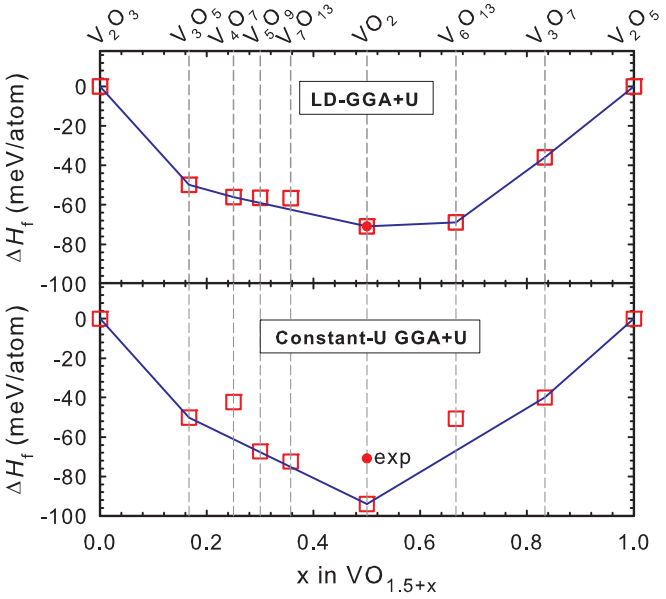

FIG. 7. (Color online) The convex hulls calculated by LD-GGA+U and constant-U GGA+U for the vanadium-oxygen system in the region $x = 0$–1 in $VO_{1.5+x}$. This region covers mixed-valence V-O compounds and VO_2, where valance of vanadium ranges from 3+ to 5+. Formation enthalpies are given with respect to V_2O_3 ($x = 0$) and V_2O_5 ($x = 1$).

dependence on U and does not match with the experimental value at any U (see the Supplemental Material [39]). Thus, no such constant U value can be found for V that "reasonably" represents the thermochemistry of all phases spanning the range from V^{3+} to V^{5+} in the V-O system. LD-GGA+U helps overcome this shortcoming by taking the oxidation state dependence of U into account explicitly.

V. SUMMARY

In this study, we have developed a method to estimate local environment dependent U values to be used in GGA+U thermochemistry. These U values have an explicit dependence on the oxidation state and the coordinating ligand of the transition metal in a compound. We have applied the method to calculate such U values for common oxidation states of oxides and fluorides of 3d-block metals Ti, V, Cr, Mn, Fe, Co, and Ni using a training set composed mainly of binary compounds. In the presented method, the total energy compatibility among calculations with different U values of a metal is realized by implementing the GGA/GGA+U mixing scheme by Jain *et al.* [38]. We have validated the transferability of the LD-GGA+U parameters acquired from binary compounds to similar local environments in different compounds by calculating the formation enthalpies of a test set of 52 3d-metal bearing oxides (not included in fit set). For this test set, our method yields a MAE of 19 meV/atom relative to experimental data upon predicting the formation enthalpies, which is a significantly lower error than other methods, and is very close to the average experimental uncertainty of approximately 10 meV/atom in the same test set.

We have further demonstrated that LD-GGA+U can help overcome deficiencies of using a constant U in certain redox processes. Predictions of Li-battery voltages and stabilities of mixed-valence compounds are particularly improved with LD-GGA+U, especially in systems such as Li_xCoO_2 and $VO_{1.5+x}$ where a single U value cannot adequately describe the thermochemistry in the entire oxidation state range of the transition metal. Calculation of U values with LD-GGA+U requires only standard GGA+U calculations and experimental formation enthalpies and, therefore, it can be easily applied to new systems. Formation enthalpy calculations using the LD-GGA+U parameters are also straightforward, and can be readily implemented in high-throughput DFT databases to supplement current GGA+U/energy correction schemes.

ACKNOWLEDGMENTS

The authors gratefully acknowledge helpful discussions with Professor D. Morgan, Dr. S. Hao, Dr. J. Bhattacharya, S. Kirklin, D. Snydacker, Z. Lu, and S. Kim. M.A. and C.W. were supported by The Dow Chemical Company. C.W. was also supported by the US Department of Energy under Grant No. DE-FG02-07ER46433. This research used resources of the National Energy Research Scientific Computing Center, a DOE Office of Science User Facility supported by the Office of Science of the US Department of Energy under Contract No. DE-AC02-05CH11231.

APPENDIX A

We observed that U dependence of the GGA+U total energy is generally well described with a quadratic relation. Thus, for convenience, inserting such expansions for $E_{MX_{a/x}}(U^X_{M^{a+}})$ and $E_{MY_{b/y}}(U^Y_{M^{b+}})$ about $\bar{U}_i$ into Eq. (3), we obtain

$$\bar{U}_i - \frac{\alpha^X_{M^{a+}} U^X_{M^{a+}} + \alpha^Y_{M^{b+}} U^Y_{M^{b+}}}{\alpha^X_{M^{a+}} + \alpha^Y_{M^{b+}}} - \frac{1}{\alpha^X_{M^{a+}} + \alpha^Y_{M^{b+}}} \times \left[\beta^X_{M^{a+}}\left(\bar{U}_i - U^X_{M^{a+}}\right)^2 + \beta^Y_{M^{b+}}\left(\bar{U}_i - U^Y_{M^{b+}}\right)^2\right] = 0, \tag{A1}$$

where $\alpha^X_{M^{a+}} = (dE_{MX_{a/x}}/dU)_{\bar{U}_i}$ and $\beta^X_{M^{a+}} = \frac{1}{2}(d^2E_{MX_{a/x}}/dU^2)_{\bar{U}_i}$, and $\alpha^Y_{M^{b+}}$ and $\beta^Y_{M^{b+}}$ are also defined similarly. These coefficients are extracted from the variation of GGA+U total energies with U, and $\bar{U}_i$ is determined by the method of Wang *et al.* [16] as in Eq. (2). Then, $U^X_{M^{a+}}$ and $U^Y_{M^{b+}}$ remain as the only unknowns in Eq. (A1), which can be directly employed in the optimization procedure of calculating U values with LD-GGA+U.

APPENDIX B

Equation (8) provides a convenient basis also for calculating $\bar{U}_i$ by the method of Wang *et al.* [16]. This can simply be shown by converting Eq. (8) to a function of U as

$$\delta\mu^X_{M^{a+}} = E_{MX_{a/x}}(U) - \mu^{\mathrm{GGA}}_M - \frac{a}{2x}\mu^{\mathrm{fit}}_{X_2} - \Delta H^{\mathrm{expt}}_f[MX_{a/x}]. \tag{B1}$$

For each $MX_{a/x}/MY_{b/y}$ pair, $\bar{U}_i$ can then be found at the intersection point of $\delta\mu^X_{M^{a+}}(U)$ and $\delta\mu^Y_{M^{b+}}(U)$, i.e., at $\delta\mu^X_{M^{a+}}(\bar{U}_i) = \delta\mu^Y_{M^{b+}}(\bar{U}_i)$. This is equivalent to finding $\bar{U}_i$ at

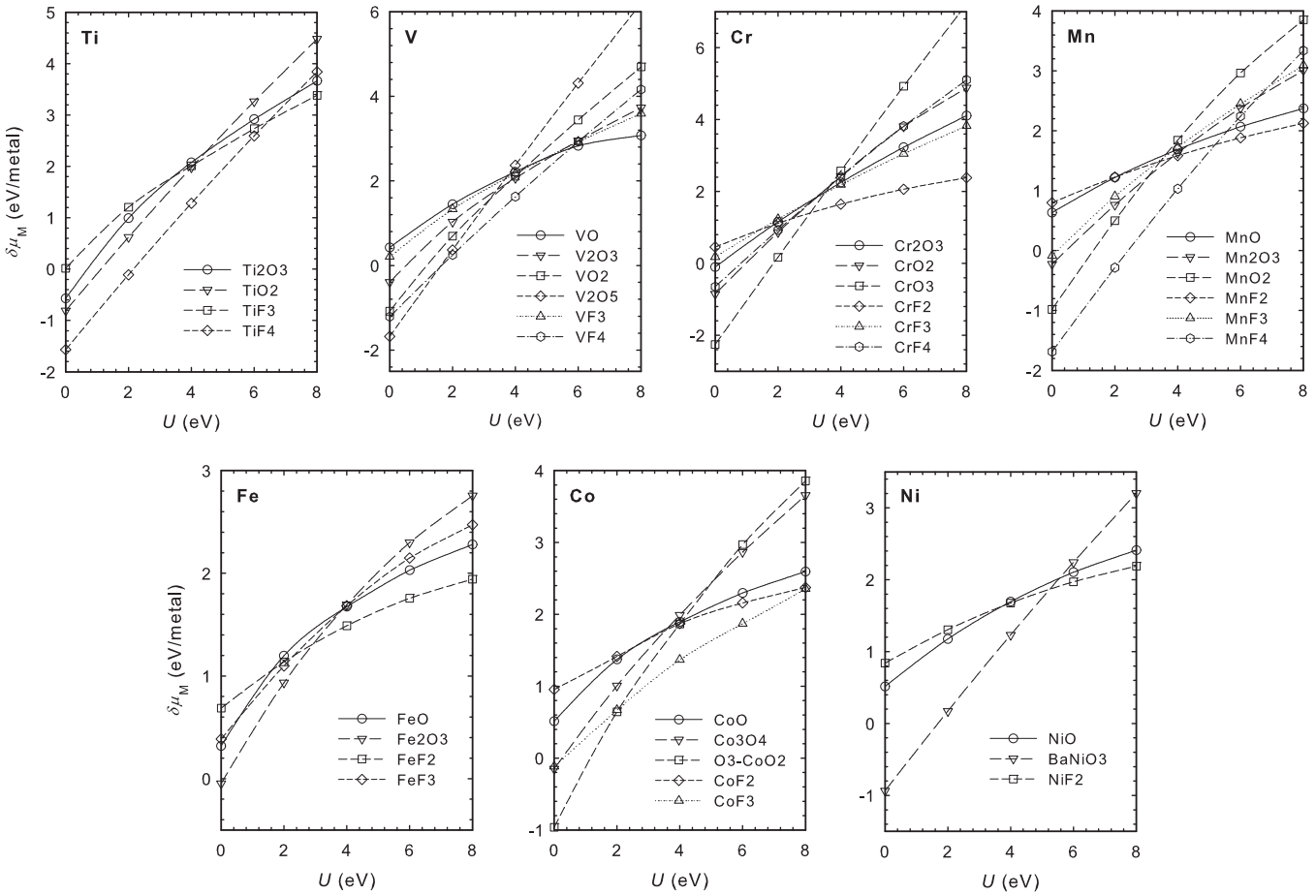

FIG. 8. The $\delta\mu^X_{M^{a+}}(U)$ functions of compounds included in our U-prediction calculations. Intersection point of any two $\delta\mu^X_{M^{a+}}$ curves corresponds to $\bar{U}$ of the reaction between the corresponding compounds.

$\Delta H_i^{\rm calc}(\bar{U}_i) = \Delta H_i^{\rm expt}$ as described by Eq. (2). We show the calculated $\delta\mu^X_{M^{a+}}(U)$ of compounds employed in U-prediction calculations in Fig. 8, where in each panel, every intersection point corresponds to $\bar{U}_i$ of a reaction i. Once the unique LD-U values are determined, we also find $\Delta\mu^X_{M^{a+}}$ from these plots as $\Delta\mu^X_{M^{a+}} = \delta\mu^X_{M^{a+}}(U^X_{M^{a+}})$.

To find the LD-U values, we first need to calculate the $\bar{U}_i$; therefore, there should exist a solution to Eq. (2) for reaction i to have a $\bar{U}_i$. While a reasonable $\bar{U}_i$ can be obtained for almost all reactions, there are a few cases where one may not be able to find a $\bar{U}_i$. In the first case, if $U^X_{M^{a+}}$ and $\bar{U}_i$ are widely apart such as $U^X_{M^{a+}} \ll \bar{U}_i$ or $U^X_{M^{a+}} \gg \bar{U}_i$, the $\bar{U}_i$ that we find may be unphysical. In other words, at a $\bar{U}_i$ that largely deviates from $U^X_{M^{a+}}$, one might also largely deviate from the presumably ideal electronic description of the compound $MX_{a/x}$ obtained at $U^X_{M^{a+}}$. For example, in case of the reactions of cobalt compounds, all $\bar{U}_i$ values are in reasonable ranges, except for the $\bar{U}_i$ values involving CoF_3 (see Fig. 8). The redox reaction between CoF_2 and CoF_3 has a $\bar{U}_i$ around 8 eV. Given all other reactions that CoF_2 participates have much smaller $\bar{U}_i$, CoF_3 is expected to have a U larger than that of CoF_2, and above 8 eV. Therefore, for all other reactions of CoF_3, we have $U^{\rm F}_{\rm Co^{3+}} \gg \bar{U}_i$, and no $\bar{U}_i$ could be found in a meaningful range. Accordingly, we allow CoF_3 to participate the fitting only through its reaction with CoF_2, which has a minimal effect on the U values of the rest of the Co compounds. For certain reactions, one may not be able to find a $\bar{U}_i$ by fitting to the experimental enthalpy. This is often the case when the variations of $\partial E_{MX_{a/x}}/\partial U$ and $\partial E_{MY_{b/y}}/\partial U$ with U are very similar for the respective compounds in Eq. (1). Fortunately, among all reactions in the form of Eq. (1) considered in this work, only a few reactions had to be excluded from the fit set (in addition to the CoF_3 example above) due to aforementioned reasons. These reactions are Mn_2O_3/MnF_3, MnO_2/MnF_4, TiO_2/TiF_4, VO_2/VF_4, and V_2O_5/VF_4. LD-GGA+U framework provides the flexibility of removing such reactions from the fit set because as long as the number of $\bar{U}_i$ values that we know is more than or equal to the number of unknown $U^X_{M^{a+}}$, we can find those $U^X_{M^{a+}}$ values.

The calculation of $U^X_{M^{a+}}$ values with the LD-GGA+U method is a straightforward procedure because to include a compound of M in the calculation, we only need its experimental formation energy and a series of regular GGA+U total energy calculations as a function of U. Nevertheless, LD-GGA+U is an empirical approach based on fitting to experimental data, and the $\bar{U}_i$ values used to derive $U^X_{M^{a+}}$ show a strong dependence on the data input. Therefore, an assessment of the available experimental and computational data is essential for the application of LD-GGA+U. While selecting the experimental formation enthalpies, we note that

data with minimum uncertainty should be preferred, and furthermore, the enthalpy difference between 0 and 298 K should not be neglected (see Sec. III B). We estimate that the average 0–298 K formation enthalpy difference to be over 10 meV/atom using a sample set of compounds from JANAF (see the Supplemental Material [39]). In addition, magnetic structure (beyond ferromagnetic spins) is also an important factor to take into account in GGA+U calculations as we list in Table I because it can considerably alter the obtained GGA+U total energy (see Sec. III A).

[1] M. K. Aydinol, A. F. Kohan, G. Ceder, K. Cho, and J. Joannopoulos, Phys. Rev. B **56**, 1354 (1997).
[2] C. Wolverton and A. Zunger, Phys. Rev. Lett. **81**, 606 (1998).
[3] S. Kirklin, B. Meredig, and C. Wolverton, Adv. Energy Mater. **3**, 252 (2013).
[4] F. Zhou, M. Cococcioni, C. A. Marianetti, D. Morgan, and G. Ceder, Phys. Rev. B **70**, 235121 (2004).
[5] J. Reed and G. Ceder, Electrochem. Solid State Lett. **5**, A145 (2002).
[6] M. K. Y. Chan, C. Wolverton, and J. P. Greeley, J. Am. Chem. Soc. **134**, 14362 (2012).
[7] A. R. Akbarzadeh, V. Ozoliņš, and C. Wolverton, Adv. Mater. **19**, 3233 (2007).
[8] W. Q. Sun, C. Wolverton, A. R. Akbarzadeh, and V. Ozoliņš, Phys. Rev. B **83**, 064112 (2011).
[9] C. Wolverton, D. J. Siegel, A. R. Akbarzadeh, and V. Ozoliņš, J. Phys.: Condens. Matter **20**, 064228 (2008).
[10] M. Arroyo y de Dompablo and G. Ceder, J. Alloys Compd. **364**, 6 (2004).
[11] J. W. Doak and C. Wolverton, Phys. Rev. B **86**, 144202 (2012).
[12] C. Wolverton, Modell. Simul. Mater. Sci. Eng. **8**, 323 (2000).
[13] J. Greeley and M. Mavrikakis, Nat. Mater. **3**, 810 (2004).
[14] G. Jones, J. Jakobsen, S. Shim, J. Kleis, M. Andersson, J. Rossmeisl, F. Abildpedersen, T. Bligaard, S. Helveg, and B. Hinnemann, J. Catal. **259**, 147 (2008).
[15] J. P. Perdew and A. Zunger, Phys. Rev. B **23**, 5048 (1981).
[16] L. Wang, T. Maxisch, and G. Ceder, Phys. Rev. B **73**, 195107 (2006).
[17] S. Lutfalla, V. Shapovalov, and A. T. Bell, J. Chem. Theory Comput. **7**, 2218 (2011).
[18] V. L. Chevrier, S. P. Ong, R. Armiento, M. K. Y. Chan, and G. Ceder, Phys. Rev. B **82**, 075122 (2010).
[19] G. Hautier, S. P. Ong, A. Jain, C. J. Moore, and G. Ceder, Phys. Rev. B **85**, 155208 (2012).
[20] V. I. Anisimov, J. Zaanen, and O. K. Andersen, Phys. Rev. B **44**, 943 (1991).
[21] A. I. Liechtenstein, V. I. Anisimov, and J. Zaanen, Phys. Rev. B **52**, R5467 (1995).
[22] V. I. Anisimov, J. Phys.: Condens. Matter **9**, 767 (1997).
[23] S. L. Dudarev, G. A. Botton, S. Y. Savrasov, C. J. Humphreys, and A. P. Sutton, Phys. Rev. B **57**, 1505 (1998).
[24] M. Cococcioni and S. de Gironcoli, Phys. Rev. B **71**, 035105 (2005).
[25] V. I. Anisimov and O. Gunnarsson, Phys. Rev. B **43**, 7570 (1991).
[26] O. Gunnarsson, O. K. Andersen, O. Jepsen, and J. Zaanen, Phys. Rev. B **39**, 1708 (1989).
[27] N. J. Mosey and E. A. Carter, Phys. Rev. B **76**, 155123 (2007).
[28] N. J. Mosey, P. Liao, and E. A. Carter, J. Chem. Phys. **129**, 014103 (2008).
[29] F. Aryasetiawan, M. Imada, A. Georges, G. Kotliar, S. Biermann, and A. I. Lichtenstein, Phys. Rev. B **70**, 195104 (2004).
[30] K. Karlsson, F. Aryasetiawan, and O. Jepsen, Phys. Rev. B **81**, 245113 (2010).
[31] F. Aryasetiawan, K. Karlsson, O. Jepsen, and U. Schönberger, Phys. Rev. B **74**, 125106 (2006).
[32] G. Rollmann, A. Rohrbach, P. Entel, and J. Hafner, Phys. Rev. B **69**, 165107 (2004).
[33] D. O. Scanlon, A. Walsh, B. J. Morgan, and G. W. Watson, J. Phys. Chem. C **112**, 9903 (2008).
[34] C. Loschen, J. Carrasco, K. M. Neyman, and F. Illas, Phys. Rev. B **75**, 035115 (2007).
[35] S. Grindy, B. Meredig, S. Kirklin, J. E. Saal, and C. Wolverton, Phys. Rev. B **87**, 075150 (2013).
[36] F. Zhou, M. Cococcioni, K. Kang, and G. Ceder, Electrochem. Commun. **6**, 1144 (2004).
[37] C. Franchini, R. Podloucky, J. Paier, M. Marsman, and G. Kresse, Phys. Rev. B **75**, 195128 (2007).
[38] A. Jain, G. Hautier, S. P. Ong, C. J. Moore, C. C. Fischer, K. A. Persson, and G. Ceder, Phys. Rev. B **84**, 045115 (2011).
[39] See Supplemental Material at http://link.aps.org/supplemental/10.1103/PhysRevB.90.115105 for (i) a test for the accuracy of the procedure of extrapolating the 298-K experimental formation enthalpies to 0 K, and (ii) a series of GGA+U reaction enthalpy calculations to test whether a common U value can be found for all oxidation states in the V-O system.
[40] N. Blümer and E. V. Gorelik, Phys. Rev. B **87**, 085115 (2013).
[41] H. U. R. Strand, A. Sabashvili, M. Granath, B. Hellsing, and S. Östlund, Phys. Rev. B **83**, 205136 (2011).
[42] N. Blümer, Ph.D. thesis, Universität Augsburg, 2003.
[43] V. Stevanović, S. Lany, X. Zhang, and A. Zunger, Phys. Rev. B **85**, 115104 (2012).
[44] S. Lany, Phys. Rev. B **78**, 245207 (2008).
[45] A. Jain, G. Hautier, C. J. Moore, S. Ping Ong, C. C. Fischer, T. Mueller, K. A. Persson, and G. Ceder, Comput. Mater. Sci. **50**, 2295 (2011).
[46] A. Jain, S. P. Ong, G. Hautier, W. Chen, W. D. Richards, S. Dacek, S. Cholia, D. Gunter, D. Skinner, G. Ceder, and K. A. Persson, APL Mater. **1**, 011002 (2013).
[47] J. E. Saal, S. Kirklin, M. Aykol, B. Meredig, and C. Wolverton, JOM **65**, 1501 (2013).
[48] G. Kresse and J. Hafner, Phys. Rev. B **47**, 558 (1993).
[49] G. Kresse and J. Hafner, Phys. Rev. B **49**, 14251 (1994).
[50] G. Kresse and J. Furthmüller, Comput. Mater. Sci. **6**, 15 (1996).
[51] G. Kresse and J. Furthmüller, Phys. Rev. B **54**, 11169 (1996).
[52] J. P. Perdew, K. Burke, and M. Ernzerhof, Phys. Rev. Lett. **77**, 3865 (1996).

[53] J. P. Perdew, K. Burke, and M. Ernzerhof, Phys. Rev. Lett. **78**, 1396 (1997).
[54] P. E. Blöchl, Phys. Rev. B **50**, 17953 (1994).
[55] A. van de Walle, M. Asta, and G. Ceder, CALPHAD: Comput. Coupling Phase Diagrams Thermochem. **26**, 539 (2002).
[56] M. Wang, A. Navrotsky, S. Venkatraman, and A. Manthiram, J. Electrochem. Soc. **152**, J82 (2005).
[57] K. Jacob and J. Hajra, Bull. Mater. Sci. **9**, 37 (1987).
[58] A. Azad and O. Sreedharan, J. Appl. Electrochem. **17**, 949 (1987).
[59] G. Johnson, J. Chem. Thermodyn. **13**, 465 (1981).
[60] R. Hoppe, B. Müller, J. Burgess, R. D. Peacock, and R. Sherry, J. Fluorine Chem. **16**, 189 (1980).
[61] J. DiCarlo, I. Yazdi, A. J. Jacobson, and A. Navrotsky, J. Solid State Chem. **109**, 223 (1994).
[62] P. A. G. O'Hare, G. K. Johnson, M. Ader, W. N. Hubbard, D. R. Fredrickson, F. A. Cafasso, and L. Burris, Argonne National Laboratory Technical Report No. ANL-76-102, 1976.
[63] W. Roth, Phys. Rev. **110**, 1333 (1958).
[64] W. Roth, J. Phys. Chem. Solids **25**, 1 (1964).
[65] R. Erickson, Phys. Rev. **90**, 779 (1953).
[66] E. Wollan, H. Child, W. Koehler, and M. Wilkinson, Phys. Rev. **112**, 1132 (1958).
[67] L. M. Corliss, J. M. Hastings, R. Nathans, and G. Shirane, J. Appl. Phys. **36**, 1099 (1965).
[68] V. Sivakumar, C. A. Ross, N. Yabuuchi, Y. Shao-Horn, K. Persson, and G. Ceder, J. Electrochem. Soc. **155**, P83 (2008).
[69] T. Chatterji and T. C. Hansen, J. Phys.: Condens. Matter **23**, 276007 (2011).
[70] Z. Mazej, J. Darriet, J. Grannec, K. Lutar, A. Tressaud, and B. Zemva, J. Fluorine Chem. **99**, 25 (1999).
[71] M. Regulski, R. Przenioso, I. Sosnowska, D. Hohlwein, and R. Schneider, J. Alloys Compd. **362**, 236 (2004).
[72] Y. Akio, J. Phys. Soc. Jpn. **14**, 807 (1959).
[73] R. M. Moon, T. Riste, W. C. Koehler, and S. C. Abrahams, J. Appl. Phys. **40**, 1445 (1969).
[74] D. Adler, Rev. Mod. Phys. **40**, 714 (1968).
[75] E. Balcar and S. Lovesey, J. Phys.: Condens. Matter **14**, 10281 (2002).
[76] B. Meredig, A. Thompson, H. A. Hansen, C. Wolverton, and A. van de Walle, Phys. Rev. B **82**, 195128 (2010).
[77] A. Belsky, M. Hellenbrandt, V. L. Karen, and P. Luksch, Acta Crystallogr., Sect. B: Struct. Sci. **58**, 364 (2002).
[78] I. D. Brown and D. Altermatt, Acta Crystallogr., Sect. B: Struct. Sci. **B41**, 244 (1985).
[79] K. Momma and F. Izumi, J. Appl. Crystallogr. **41**, 653 (2008).
[80] M. W. Chase, C. A. Davies, J. R. Downey, D. J. Frurip, R. A. McDonald, and A. N. Syverud, J. Phys. Chem. Ref. Data. **14**, Suppl. 1 (1985).
[81] O. Kubaschewski, C. Alcock, and P. Spencer, *Materials Thermochemistry*, 6th ed. (Pergamon, New York, 1993).
[82] I. Barin, *Thermochemical Data of Pure Substances*, 3rd ed. (VCH, Weinheim, 1995).
[83] D. Wagman, W. Evans, V. Parker, R. Schumm, I. Halow, S. Bailey, K. Churney, and R. Nuttall, J. Phys. Chem. Ref. Data **11**, Suppl. 2 (1982).
[84] J. Höwing, T. Gustafsson, and J. O. Thomas, Acta Crystallogr., Sect. B: Struct. Sci. **59**, 747 (2003).
[85] M. E. Arroyo-de Dompablo, A. Morales-García, and M. Taravillo, J. Chem. Phys. **135**, 054503 (2011).
[86] I. V. Solovyev and P. H. Dederichs, Phys. Rev. B **49**, 6736 (1994).
[87] I. Solovyev, N. Hamada, and K. Terakura, Phys. Rev. B **53**, 7158 (1996).
[88] E. R. Ylvisaker, W. E. Pickett, and K. Koepernik, Phys. Rev. B **79**, 035103 (2009).
[89] D. Khan and R. Erickson, Phys. Rev. B **1**, 2243 (1970).
[90] J. van Elp, J. L. Wieland, H. Eskes, P. Kuiper, G. A. Sawatzky, F. M. F. de Groot, and T. S. Turner, Phys. Rev. B **44**, 6090 (1991).
[91] T. Motohashi, Y. Katsumata, T. Ono, R. Kanno, M. Karppinen, and H. Yamauchi, Chem. Mater. **19**, 5063 (2007).
[92] G. Amatucci, J. Tarascon, and L. Klein, J. Electrochem. Soc. **143**, 1114 (1996).
[93] T. Chatterji, B. Ouladdiaf, and T. C. Hansen, J. Phys.: Condens. Matter **22**, 096001 (2010).
[94] A. E. Bocquet, T. Mizokawa, K. Morikawa, A. Fujimori, S. R. Barman, K. Maiti, D. D. Sarma, Y. Tokura, and M. Onoda, Phys. Rev. B **53**, 1161 (1996).
[95] B. Chamberland, Crit. Rev. Solid State Mater. Sci. **7**, 1 (1977).
[96] J. M. D. Coey and M. Venkatesan, J. Appl. Phys. **91**, 8345 (2002).
[97] R. Zimmermann, P. Steiner, R. Claessen, F. Reinert, S. Hfner, P. Blaha, and P. Dufek, J. Phys.: Condens. Matter **11**, 1657 (1999).
[98] E. Krén, P. Szabó, and G. Konczos, Phys. Lett. **19**, 103 (1965).
[99] A. Chainani, T. Yokoya, T. Morimoto, T. Takahashi, and S. Todo, Phys. Rev. B **51**, 17976 (1995).
[100] T. Chatterji, G. N. Iles, B. Ouladdiaf, and T. C. Hansen, J. Phys.: Condens. Matter **22**, 316001 (2010).
[101] A. K. Cheetham and D. A. O. Hope, Phys. Rev. B **27**, 6964 (1983).
[102] W. Strehlow and E. Cook, J. Phys. Chem. Ref. Data **2**, 163 (1973).
[103] M. Regulski, R. Przenioslo, I. Sosnowska, and J.-U. Hoffmann, Phys. Rev. B **68**, 172401 (2003).
[104] K. Lutar, A. Jesih, and B. Žemva, Polyhedron **7**, 1217 (1988).
[105] H. J. Kulik and N. Marzari, J. Chem. Phys. **135**, 194105 (2011).
[106] J. Heyd, G. E. Scuseria, and M. Ernzerhof, J. Chem. Phys. **118**, 8207 (2003).
[107] A. V. Krukau, O. A. Vydrov, A. F. Izmaylov, and G. E. Scuseria, J. Chem. Phys. **125**, 224106 (2006).
[108] H. Xia, L. Lu, Y. S. Meng, and G. Ceder, J. Electrochem. Soc. **154**, A337 (2007).
[109] C. Wolverton and A. Zunger, J. Electrochem. Soc. **145**, 2424 (1998).
[110] M. Ménétrier, D. Carlier, M. Blangero, and C. Delmas, Electrochem. Solid State Lett. **11**, A179 (2008).
[111] T. Motohashi, T. Ono, Y. Sugimoto, Y. Masubuchi, S. Kikkawa, R. Kanno, M. Karppinen, and H. Yamauchi, Phys. Rev. B **80**, 165114 (2009).
[112] Y. Takahashi, N. Kijima, K. Tokiwa, T. Watanabe, and J. Akimoto, J. Phys.: Condens. Matter **19**, 436202 (2007).
[113] T. Schmitt, A. Augustsson, L.-C. Duda, J. Nordgren, and J. Höwing, J. Appl. Phys. **95**, 6444 (2004).
[114] N. A. Chernova, M. Roppolo, A. C. Dillon, and M. S. Whittingham, J. Mater. Chem. **19**, 2526 (2009).

[115] J. Höwing, T. Gustafsson, and J. O. Thomas, Acta Crystallogr., Sect. B: Struct. Sci. **60**, 382 (2004).
[116] R. E. Doe, K. A. Persson, Y. S. Meng, and G. Ceder, Chem. Mater. **20**, 5274 (2008).
[117] F. Badway, N. Pereira, F. Cosandey, and G. G. Amatucci, J. Electrochem. Soc. **150**, A1209 (2003).
[118] F. Badway, F. Cosandey, N. Pereira, and G. G. Amatucci, J. Electrochem. Soc. **150**, A1318 (2003).
[119] P. Liu, J. Vajo, J. Wang, W. Li, and J. Liu, J. Phys. Chem. C **116**, 6467 (2012).
[120] N. Yamakawa, M. Jiang, B. Key, and C. P. Grey, J. Am. Chem. Soc. **131**, 10525 (2009).
[121] M. Zhou, L. Zhao, A. Kitajou, S. Okada, and J.-i. Yamaki, J. Power Sources **203**, 103 (2012).
[122] F. Wang, R. Robert, N. A. Chernova, N. Pereira, F. Omenya, F. Badway, X. Hua, M. Ruotolo, R. Zhang, L. Wu, V. Volkov, D. Su, B. Key, M. S. Whittingham, C. P. Grey, G. G. Amatucci, Y. Zhu, and J. Graetz, J. Am. Chem. Soc. **133**, 18828 (2011).
[123] H. Wriedt, Bull. Alloy Phase Diagrams **10**, 271 (1989).
[124] H. Katzke, P. Tolédano, and W. Depmeier, Phys. Rev. B **68**, 024109 (2003).
[125] Compounds V_6O_{11} and V_8O_{15}, which undergo phase transitions below room temperature as reported in K. Nagasawa, Y. Bando, and T. Takada, Bull. Inst. Chem. Res., Kyoto Univ. **49**, 322 (1971) are not included in Fig. 7, because the corresponding low-temperature crystal structure information below transition temperatures is not available.
[126] A. Chippindale and P. Dickens, J. Mater. Chem. **2**, 601 (1992).
[127] K. Jacob and G. Rajitha, J. Chem. Thermodyn. **43**, 51 (2011).
[128] P. A. Romodanovskii, N. G. Dmitrieva, S. N. Gridchin, and P. N. Vorobev, Russ. J. Inorg. Chem. **56**, 1491 (2011).
[129] R. L. Schmidt, Pacific Northwest Laboratory Technical Report No. PNL-4881, 1984.
[130] A. Mukhopadhyay, A. Bhattacharya, and L. Mohanty, Contrib. Mineral. Petrol. **110**, 346 (1992).